Prediction Skill of GEFSv12 for Southwest Summer Monsoon Rainfall and Associated Extreme Rainfall Events on Extended Range Scale over India

M. M. NAGESWARARAO,[a,b] YUEJIAN ZHU,[b] AND VIJAY TALLAPRAGADA[b]

[a] *CPAESS, University Corporation for Atmospheric Research, Boulder, Colorado*
[b] *NOAA/NWS/NCEP/EMC, College Park, Maryland*

(Manuscript received 16 November 2021, in final form 30 March 2022)

ABSTRACT: Indian summer monsoon rainfall (ISMR) from June to September (JJAS) contributes 80% of the total annual rainfall in India and controls the agricultural productivity and economy of the country. Extreme rainfall (ER) events are responsible for floods that cause widespread destruction of infrastructure, economic damage, and loss of life. A forecast of the ISMR and associated ER events on an extended range (beyond the conventional one-week lead time) is vital for the agronomic economy of the country. In September 2020, NOAA/NCEP implemented Global Ensemble Forecast System, version 12 (GEFSv12) for various risk management applications. It has generated consistent reanalysis and reforecast data for the period 2000–19. In the present study, the Raw-GEFSv12 with day-1–16 lead-time rainfall forecasts are calibrated using the quantile (QQ) mapping technique against Indian Monsoon Data Assimilation and Analysis (IMDAA) for further improvement. The present study evaluated the prediction skill of Raw and QQ-GEFSv12 for ISMR and ER events over India by using standard skill metrics. The results suggest that the ISMR patterns from Raw and QQ-GEFSv12 with (lead) day 1–16 are similar to IMDAA. However, Raw-GEFSv12 has a dry bias in most parts of prominent rainfall regions. The low- to medium-intensity rainfall events from Raw-GEFSv12 is remarkably higher than the IMDAA, while high- to very-high-intensity rainfall events from Raw-GEFSv12 are lower than IMDAA. The prediction skill of Raw-GEFSv12 in depicting ISMR and associated ER events decreased with lead time, while the prediction skill is almost equal for all lead times with marginal improvement after calibration.

KEYWORDS: Monsoons; Extreme events; Forecast verification/skill; Postprocessing; Probability forecasts/models/distribution; Rainfall; Ensembles; Probabilistic Quantitative Precipitation Forecasting (PQPF)

1. Introduction

In India, the Indian summer monsoon [June–September (JJAS) hereafter ISM] and northeast monsoon [October–December (OND)] are the major rainfall seasons. However, the JJAS season alone contributed 80% of the annual rainfall over India, and for most of the country except for south peninsular India (SPI), maximum rainfall occurred during JJAS. The SPI (Tamil Nadu, Rayalaseema, Karnataka, etc.) receives maximum rainfall during OND. In India, there are many years with a flood (strong monsoon) receiving excess or drought (weak monsoon) with deficient rainfall during the seasons, respectively. Goswami and Chakravorty (2017) found the variability in ISMR is highly determined by internal dynamics arising from ocean–atmosphere–land interactions and remote teleconnections via different climate modes. Directly or indirectly, 49% of employment in India is involved in the agriculture and allied sectors. Extreme rainfall (ER) events are responsible for floods that cause widespread destruction of infrastructure, economic damage, and the loss of lives across the world, and its high over Asia. Adhikari et al. (2010) study found around 247 000 fatalities worldwide due to flood events from 1998 to 2008. Many studies (Rosenzweig et al. 2002; Sen Roy and Balling 2004; Zhai et al. 2005; Goswami et al. 2006; Wang et al. 2006; Hegerl et al. 2007; Endo et al. 2009; Krishnamurthy et al. 2009; Rosenberg et al. 2010; Yao et al. 2010; Mirza 2011; Keller and Atzl 2014; Vogel et al. 2019) showed a consistent intensification of ER events in the warm tropical environment, and it is remarkably high in many parts of the Asian continent. In recent decades, the ER events in various parts of India significantly amplified during different seasons (Sen Roy and Balling 2004; Nageswararao et al. 2016, 2019a,b; Barde et al. 2020). According to the International Disaster Database, the economic loss caused by floods in India is about $3 billion per year in India is 10% of the global financial losses of $30 billion per year (Jonkman 2005; Mirza 2011). Therefore, there is a demand for understanding, monitoring, and predicting extreme weather events over India for the country's sustainability, especially in this present global warming era (Vitart et al. 2012).

Most of the ER events over India occur during ISM and are associated with monsoon depressions over the Bay of Bengal. Further, they propagate northwest or westward toward the inland. These systems are associated with a mix of barotropic and baroclinic instabilities and interact with the mean monsoonal flow (Gadgil 2003). In the active phase of the monsoon, ER events occurred in most parts of India, including the Western Ghats, northeast, and central region of the country, but there are spells of little or no rainfall within the JJAS. Several studies (Rao 1976; George 1956; Mukherjee et al. 1978; Mukherjee 1980; Francis and Gadgil 2006) found that the small-scale vortices embedded with offshore troughs/convective systems/bands over the west coast regions with

Supplemental information related to this paper is available at the Journals Online website: https://doi.org/WAF-D-21-0184.s1.

Corresponding author: Yuejian Zhu, Yuejian.Zhu@noaa.gov

DOI: 10.1175/WAF-D-21-0184.1

mesoscale vortices embedded in larger-scale systems over the Arabian Sea led to ER events over this region.

The orographic features over the west coast and northeast India and the movement of synoptic-scale systems from the Bay of Bengal region to the central parts of India also contribute to the ER events over those regions (Rao 1976; Soman and Krishna Kumar 1990; Gadgil 2000; Sikka 2006; Pattanaik 2007). These ER events with daily rainfall at some stations over the west coast and other parts of India cause extensive damage to life and property every year during JJAS through landslides and flash floods. They can impact the society, environment, and economy of the country significantly. Several studies (Goswami et al. 2006; Rajeevan et al. 2008; Ghosh et al. 2009; Guhathakurta et al. 2011) reveal a remarkable increase in the frequency of ER events over India during ISM. The seasonal forecast of monsoon has its applicability for policymakers. Monsoon prediction in an extended range time scale is critical for optimizing planting and harvesting (Webster and Hoyos 2004). Thus, forecasting of active and break spells of monsoon on an extended range time scale from 2 to 3–4 weeks in advance is of great importance for agricultural planning (sowing, harvesting, etc.). Extended range scale forecasts are helpful for tactical adjustments to the strategic decisions made based on the long-lead seasonal forecasts. It can help in the timely review of the prevailing monsoon conditions for providing outlooks to farmers. Therefore, the accurate prediction of ISMR and ER events on this time scale at a regional level is helpful to improve flood or drought protection programs, effective water management strategies, prevent humanitarian crises, etc. Over many years, the extended range forecasts in the tropics are one of the most challenging tasks to the meteorological scientific community (Litta et al. 2007; Nayak and Ghosh 2013; Boers et al. 2014). It fills the gap between medium-range and seasonal/long-range weather forecasts. The extended range is a rugged time range weather forecasting because much of the memory of the initial atmospheric conditions on this time scale range is lost, affecting the forecast prediction skill. On the other hand, the extended range scale is not large enough for the atmospheric signal associated with the ocean anomalies to emerge over the atmospheric noise.

In recent decades, there have been impressive advances in numerical modeling and prediction of weather and climate and, in particular, substantial improvements in the skill of short and medium-range weather forecasts over extratropical regions (Stocker 2011; Bauer et al. 2015). However, prediction skill is relatively low over tropical and monsoon regions (Stocker 2011; Bauer et al. 2015). Many studies (Houze 1997; Stevens and Feingold 2009; Krishnamurti et al. 2010; Wheeler et al. 2016; Vitart et al. 2017) found the low prediction skill over tropics is mainly due to inherent complexities in numerical modeling of tropical processes dominated by interactions among atmospheric circulation, clouds, organized convection, radiation, aerosols, precipitation, moisture, and ocean–land–atmosphere feedback on different space time scales. In recent years, the efforts on numerical modeling of ISM and its variability with different scales have increased worldwide. Krishnan et al. (2011) documented the historical chronology of ISM simulation studies from the 1960s until 2011. The Monsoon Mission project of the Ministry of Earth Sciences, Govt of India, has adopted NCEP CFSv2 (Saha et al. 2014) as the primary modeling system for advancing monsoon prediction research (Rao et al. 2019). They focused on improving the ISM predictions on different time scales through improving physical parameterization of the CFSv2 model and subsequently to the improvement of model fidelity in capturing the mean and intraseasonal variability of ISM in different time scales (Abhilash et al. 2013a,b, 2014; Ganai et al. 2015, 2016, 2019; Ramu et al. 2016; Hazra et al. 2017; Abhik et al. 2017; Pokhrel et al. 2018; Mukhopadhyay et al. 2019; Saha et al. 2019; Krishna et al. 2019). The assimilation of conventional and nonconventional observation datasets as initial conditions to numerical weather forecast models conspicuously improves the prediction skill of extreme events over India (Kar et al. 2006; Routray et al. 2010; Deb et al. 2010; Ahasan et al. 2013; Dube et al. 2014; Satyanarayana and Kar 2016). The horizontal resolutions and cumulus parameterization schemes used in numerical weather forecast models also significantly impact the prediction skill of extreme rainfall events (Deb et al. 2010). In recent years, global climate models (GCMs) have been extensively used to generate extended-range predictions with positive economic value (Kar et al. 2006). Dube et al. (2014) assessed the skill of the NCMRWF NCUM model for ER events that occurred in June 2013 over Uttarakhand, India, and they found that the NCUM performed well up to 5 days ahead, with decreasing skill beyond 5 days. Satyanarayana and Kar (2016) have also done the performance evaluation of the NCMRWF NCUM model in simulating ER events over India for ISM-2014, and they found that the model has a reasonable skill to predict up to day three forecasts, but then the skill reduces with lead time afterward. Sagar et al. (2017) used three models such as the Met Office (UKMO), National Centers for Environmental Prediction (NCEP), and the European Centre for Medium-Range Weather Forecasts (ECMWF) for the simulation of 15 rainstorm events during ISM over India for the period 2007–15. They found the rainstorm events are predictable up to 5 days in advance. However, it has limitations in spatial distribution and intensity.

In September 2020, NOAA NCEP implemented a major upgrade to the Global Ensemble Forecast System (GEFSv12) to support stakeholders for subseasonal forecasts and hydrological applications. They generated consistent reforecast data for 2000–19 and are available for the public on the amazon web service (AWS, https://registry.opendata.aws/noaa-gefs/). Several studies (Kar et al. 2006; Routray et al. 2010; Deb et al. 2010; Ahasan et al. 2013; Dube et al. 2014; Satyanarayana and Kar 2016) are available on the performance evaluation of various GCMs in depicting ER events over India during ISM, but these studies are for a few ER event cases only. As of 2021, there is no study available on the performance evaluation of GEFSv12 in depicting ISMR and associated ER events on an extended range time scale over India for the long-term period (2000–19). In this study, a detailed evaluation of the prediction skill of GEFSv12 for southwest summer monsoon rainfall and associated ER events is examined for extended range scales over India. A brief description of the data and analysis procedure is given in section 2. The results are

discussed in section 3, and the broad conclusions are presented in section 4.

2. Data and methodology

The NCEP implemented the GEFSv12 in its operations on 23 September 2020 (Zhou et al. 2022). The 20 years (2000–19) reanalysis (Hamill et al. 2022) and reforecast (Guan et al. 2022) were generated accordingly to support stakeholders and applications for value-added products. The precipitation products over the Indian subcontinent for the reforecast period (2000–19) have been obtained from Amazon web services (AWS, https://noaa-gefs-retrospective.s3.amazonaws.com/index.html), which are accessible by the broader community. The reforecast data (Guan et al. 2022) was generated with every day 0000 UTC initial conditions up to the day-16 lead-time forecast, and every Wednesday, the integration is extended up to 35 days for the period 2000–19. In contrast to the current 31-member real-time forecast system, the reforecast system has a smaller ensemble size of 5 (11) members for the 16-day (35-day run). The GEFSv12 reforecast products are based on the then operational Global Forecast System version 15.1 (GFSv15.1), which uses the Geophysical Fluid Dynamics Laboratory (GFDL) FV3 Cubed-Sphere dynamical core (Lin and Rood 1997; Lin 2004; Putman and Lin 2007; Harris and Lin 2013). The horizontal resolution of the forecast system is ~25 km (C384 grid) with 64 vertical hybrid levels and the top layer centered around 0.27 hPa (~55 km). Model physics included a modified scale-aware convection parameterization scheme for reduced excessive cloud-top cooling for the model stabilization (Han and Pan 2011; Han et al. 2017) and the hybrid eddy-diffusivity mass-flux (EDMF) scheme for the vertical mixing process of the planetary boundary layer (Han et al. 2016). The cloud microphysics scheme is derived from GFDL, which includes five predicted cloud species such as cloud water, cloud ice, rain, snow, and graupel (Zhou et al. 2019, 2022). The Rapid Radiative Transfer Model (RRTM) developed at Atmospheric and Environmental Research is used for estimating the shortwave and longwave radiative fluxes (Clough et al. 2005). The convective gravity wave drag employs the scheme developed by Chun and Baik (1998), while GFS orographic gravity wave drag, and mountain blocking schemes follow Alpert et al. (1988). The SST boundary condition is derived from a two-tiered sea surface temperature (SST) and near sea surface temperature (NSST) approach that accounts for the day-to-day variability and diurnal variation of SST, respectively (Zhu et al. 2017, 2018; Li et al. 2019). The stochastic kinetic energy backscatter (SKEB; Shutts and Palmer 2004; Shutts 2005) and stochastically perturbed parameterization tendencies (SPPTs; Buizza et al. 1999; Palmer et al. 2009) have been used to represent the model's uncertainty. Additional details on the configuration of the GEFSv12 forecast system can be found in Zhou et al. (2019, 2022). To explore the prediction skill of GEFSv12 in depicting ISMR and associated various rainfall events over India, the 5-member ensemble mean of GEFSv12 precipitation is used based on the 0000 UTC daily forecasts out to 16 lead days is used during JJAS for the period 2000–19. The GEFSv12 precipitation products are available in grib2 format at 3-h intervals at 0.25° × 0.25° resolution for the first 10 days (beyond 10 days) of the forecast, while beyond 10 days available with 6-h intervals at 0.5° × 0.5° horizontal spatial resolution. Data beyond day-10 predictions are interpolated using bilinear interpolation to the day-1–10 forecast grid points at a uniform 0.25° resolution.

For a better understanding of the ISM and its variability over India, the Indian Monsoon Data Assimilation and Analysis (IMDAA), a collaborative project with the Met Office, National Centre for Medium-Range Weather Forecasting (NCMRWF), India, and the India Meteorological Department (IMD), India has recently produced a high-resolution (12-km) satellite-era regional reanalysis dataset (Ashrit et al. 2020; Indira Rani et al. 2021). This analysis dataset covers a large geographical domain (30°–120°E, 15°S–45°N) affected by ISM (Fig. 1a). Different components of the IMDAA Regional Reanalysis system are depicted in the Flowchart (Fig. 1b). IMDAA reanalysis data from 1979 to 2019 was based on an advanced data assimilation system (4D-Var) and high-resolution Unified Model of the Met Office, the observation records from India, ECMWF, and the Met Office archives (Indira Rani et al. 2021). The observations from various sources used in IMDAA with time have been illustrated in Fig. 1c. A continuous increase in the number of assimilated observations, both conventional and satellite, can be noticed with respect to time.

The IMDAA reasonably represents critical weather phenomena of each season over India, such as low-level jet and tropical easterly jet consistent with India Meteorological Department (IMD) observations and ERA5 reanalysis (Mahmood et al. 2018; Ashrit et al. 2020; Indira Rani et al. 2021). More detailed aspects of IMDAA reanalysis, including quality control and bias correction of observations, data assimilation system, land surface analysis, and verification of reanalysis products, can be found in Indira Rani et al. (2021). The IMDAA is reasonably good in depicting summer monsoon seasonal rainfall's climatological features such as climatological mean, interannual variability and coefficient of variation over the Indian domain like India Meteorological department observed analysis data (IMD-OBS) and CMORPH analysis data (see Fig. S1 in the online supplemental material). It is also good at capturing fine-scale features associated with ER episodes over complex terrain. The introduction of new observations over time with an increment of different meteorological variables and the response of the data assimilation system clearly shows the prediction skill improvement in depicting ISMR and associated ER episodes (Indira Rani et al. 2021). These studies concluded that the IMDAA high-resolution reanalysis dataset is the best choice for evaluating high-resolution dynamical models over India for further improvement of the prediction skill of the models. The IMDAA reanalysis with 3-hourly precipitation products from June to September for the reforecast period (2000–19) has been obtained from NCMRWF, Ministry of Earth Sciences, Government of India (https://rds.ncmrwf.gov.in). For evaluating the GEFSv12 performance in depicting ISMR and associated various rainfall events (as categorized by IMD) over India, 24-h accumulated/daily rainfall with the exact grid resolution are estimated from IMDAA and GEFSv12 for the study period (2000–19).

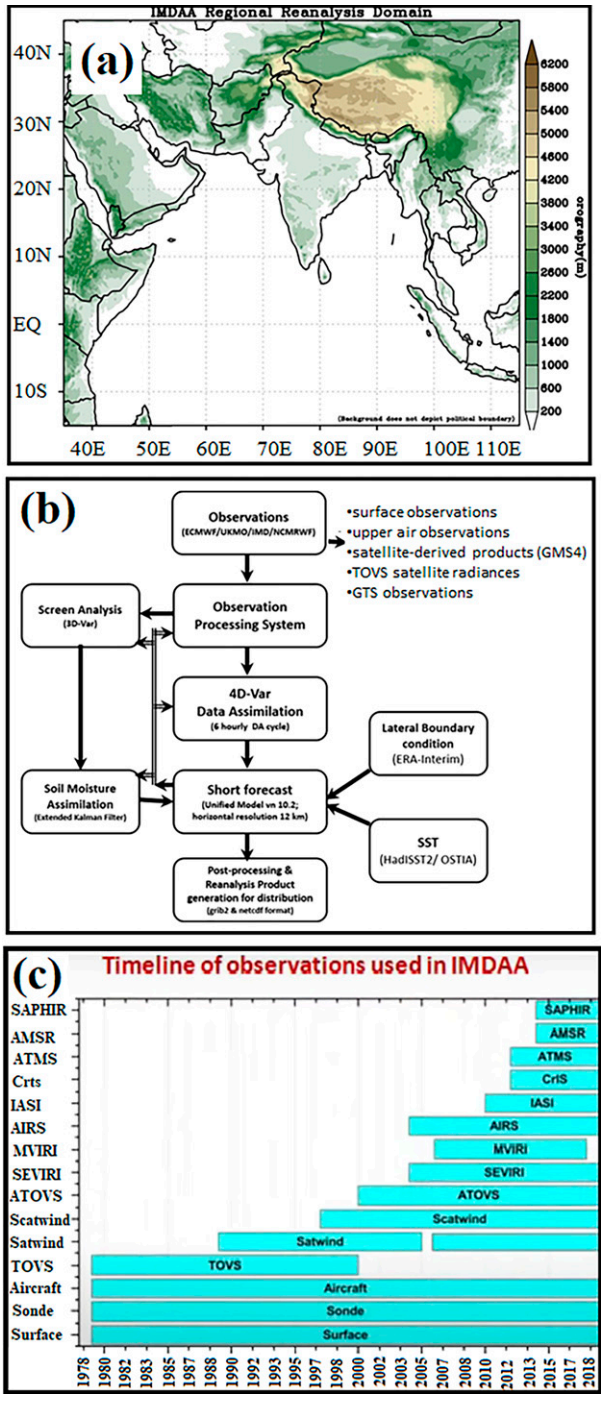

FIG. 1. (a) IMDAA Regional Reanalysis geographical domain. (b) Flowchart showing the different components of IMDAA Regional Reanalysis system. (c) The time of the observation in IMDAA (Ashrit et al. 2020; Indira Rani et al. 2021).

The numerical weather "models" raw products are not skillful at extended lead times and required statistical postprocessing to address the systematic errors to obtain more reliable and skillful forecast guidance. For further precipitation prediction skill improvement, many ensemble-based statistical postprocessing methods have been developed, e.g., "poor man's ensemble" (Ebert 2001), analog method (Hamill and Whitaker 2006), and frequency match method (FMM; Zhu and Luo 2015). In this study, the GEFSv12 rainfall raw products have been calibrated with a quantile mapping technique against IMDAA reanalysis. A quantile-based bias-correction approach helps transform rainfall simulated by GEFSv12 to statistically biased-corrected data and make it applicable for use in the impact assessment of the GEFSv12 model. This method is also referred to as "histogram equalization" and/or "rank matching" (Hamlet et al. 2002; Wood et al. 2004; Piani et al. 2010). The statistical bias-correction method employed in this study is based on the initial assumption that the gamma distribution well approximated both observed (IMDAA) and GEFSv12 simulated intensity distributions.

In the quantile mapping method, empirical probability distributions of observed and forecasted values are used. The bias-corrected output is the inverse of the cumulative distribution function (CDF) of observed values at the probability corresponding to the model output CDF at a particular value. The bias in this quantile mapping method is not calculated explicitly. The formula for the calibration for a particular lead time (t) and grid (i, j) is expressed as follows:

$$Q_{\mathrm{bc}}(i, j, t) = F^{-1}_{\mathrm{IMDAA}}\{F_{\mathrm{GEFSv12}}[Q_{\mathrm{raw}}(i, j, t)]\}.$$

Therefore, the bias-corrected value (Q_{bc}) is the inverse of the IMDAA CDF (F^{-1}_{IMDAA}) at the probability corresponding to the reforecast CDF (F_{GEFSv12}) for a given raw forecast (Q_{raw}). Here, F^{-1} is an inverse of the CDF. Thus, the procedure of the quantile mapping is a transformation between two CDFs of IMDAA and GEFSv12. In this method, the leave-one-out cross-validation procedure has been implemented. Hereafter, the Raw and calibrated outputs of GEFSv12 by using the quantile mapping method are mentioned as Raw-GEFSv12 and QQ-GEFSv12, respectively.

The gridpoint-wise climatological mean and interannual variability (IAV) of ISMR from IMDAA, Raw, and QQ-GEFSv12 (day-1, day-5, day-10, and day-15 lead times) over India for the reforecast period have been computed and the mean bias in ISMR from Raw and QQ-GEFSv12 with day-1–16 lead-time forecasts against IMDAA has been estimated. For a better understanding of GEFSv12 performance in depicting with various intensity rainfall events, the day-1, day-5, day-10, and day-15 lead-time rainfall forecast's probability distributions of 24-h accumulated rainfall from Raw and QQ-GEFSv12 during ISM over the full Indian domain (pooling all grid points) and one grid point at wet (25.5°N, 95.5°E) and dry (27.25°N, 69.5°E) regions for the study period (2000–19) have been calculated and compared with IMDAA. A scatterplot of ISM daily rainfall forecasts (day-1, day-5, day-10, and day-15 lead times) from Raw and QQ-GEFSv12 with correlation coefficient (R), slope, and regression equation against IMDAA for full Indian domain, wet and dry regions for the same period has been evaluated. To explore the spread of daily ISMR from IMDAA, Raw, and GEFSv12, a boxplot for pooling of all grid points of Indian subcontinent ISM daily

rainfall's climatological mean, interannual variability and coefficient of variation from IMDAA, Raw, and QQ-GEFSv12 for day 1, 5, 10, and 15 for the reforecast period have been analyzed.

For further analysis, various categorical daily rainfall events such as dry (<2.5 mm), wet (≥2.5 mm), very light rainfall (0.1 < VLR ≤ 2.4 mm), light rainfall (2.5 mm ≤ LR < 7.5 mm), moderate rainfall (7.6 mm ≤ MR < 35.5 mm), rather-than-heavy rainfall (35.6 mm ≤ RHR < 64.4 mm), heavy rainfall (64.5 mm ≤ HR < 124.4 mm), very heavy rainfall (124.5 mm ≤ VHR < 244.4 mm), and extremely heavy rainfall (EHR > 244.5 mm) as defined by IMD have been considered (Nageswararao et al. 2019a,b; Barde et al. 2020). The spatial distribution of wet days (≥2.5 mm day^{-1}) and high to extreme intensity heavy rainfall events (≥35.6 mm day^{-1}; RHR, HR, VHR, and EHR) over India during ISM for IMDAA, Raw, and QQ-GEFSv12 with day-1, day-5, day-10, and day-15 forecast lead times have been computed. The spread of various daily JJAS rainfall events (dry, wet, VLR, LR, MR, RHR, HR, VHR, and EHR) over India from IMDAA, Raw, and QQ-GEFSv12 with day-1, day-5, day-10, and day-15 lead times have been evaluated by using a boxplot for the reforecast period. Standard verification methods (https://www.cawcr.gov.au/projects/verification/) such as frequency bias (BIAS), probability of detection (POD), false alarm rate (FAR), success ratio (SR), threat score (TS), equitable threat score (ETS), etc. by using a contingency table for Raw and QQ-GEFSv12 with day-1, day-5, day-10, and day-15 lead-time forecasts against IMDAA in depicting various categorical ISM rainfall events over India for the reforecast period has been computed (Wilks 2011). Further, statistical categorical skill scores for wet, low-to-moderate, and high- to extremely-high-intensity rainfall events have been summarized by using a performance diagram. It exploits the geometric relationship between four measures (POD, SR, frequency bias, and TS) of dichotomous forecast performance (Roebber 2009; Huang and Luo 2017).

3. Results and discussion

The mean-bias analysis at gridpoint level reveals that the Raw-GEFSv12 with all lead times (day 1–16) has a large dry bias for ISMR over Kerala, Goa, Jammu and Kashmir, Punjab, Haryana, Delhi, Uttar Pradesh, Bihar, West Bengal, Sikkim, Assam, Meghalaya, Arunachal Pradesh, Odisha, Andhra Pradesh (the states of India can be found in Fig. S2), whereas ISMR prominently occurred (Fig. 2a). A wet bias in ISMR is noticed from Raw-GEFSv12 with all lead times over Karnataka, Telangana, Interior parts of Maharashtra, Gujarat, Madhya Pradesh, Rajasthan, Chhattisgarh, and Jharkhand. The dry and wet bias from Raw-GEFSv12 is high, particularly for day-1 lead-time forecasts and less in day-2 and day-3 lead-time forecasts then gradually increasing the biases with lead time. The mean-bias spatial pattern of ISMR from GEFSv12 is similar for all forecast lead times. Interestingly, the mean-bias error in QQ-GEFSv12 for ISMR reduced significantly for all lead times and was more consistent with respect to lead time after calibration (Fig. 2b). The reduction of dry bias or wet days after calibration is significant at a 90% confidence level in most parts of India for all forecast lead times (Fig. S3).

The Raw-GEFSv12 forecast tends to underestimate the probability of the full Indian domain ISMR for less than ~20 mm day^{-1} for all lead-time forecasts, while it has underestimated the more than ~20 mm day^{-1} for all lead-time forecasts. The underestimation for less than ~20 mm day^{-1} and the overestimation of more than ~20 mm day^{-1} of rainfall events is more for long forecast lead times (Fig. 3a). The CDF curve of daily ISMR from Raw-GEFSv12 for the day-1 forecast is closer to the observation (IMDAA) than the other lead-time forecasts. After calibration, the CDF curves from all forecast lead times were closer to the observed curve. The Raw-GEFSv12 forecast tends to overestimate the probability of daily ISMR less than 100 mm day^{-1} in the wet region. The CDF reached around 1 for less than 100 mm day^{-1} rainfall, while the CDF for less than 100 mm day^{-1} rainfall is about 0.8 from calibrated forecasts of all lead times and observation (Fig. 3b). The Raw-GEFSv12 cannot represent the more than 100 mm day^{-1} rainfall over the entire domain, and even it is not represented over predominant rainfall regions (wet regions). The calibrated forecast CDFs curve for all lead times is much closer to the observation than the Raw-GEFSv12. It is particularly better for >100 mm day^{-1}. However, there is an overestimation of the probability of ISMR for less than 100 mm day^{-1}.

In dry regions (Fig. 3c), the probability of dry days (<2.5 mm day^{-1}) is around 0.9 for the observation and calibrated forecasts for all lead-time forecasts, while the probability of dry days from Raw-GEFSv12 is low for long lead forecasts. The probability of dry days from Raw-GEFSv12 decreases with lead time while it is consistent in the calibrated forecasts and observations. The CDFs analysis concluded that the probability of the Raw-GEFSv12 was overestimated for wet days and increased with longer lead time and underestimated for high-intensity rainfall events. After calibration, both distributions and magnitudes for heavy rainfall events for all lead times are consistent with observations.

The scatterplot analysis of the entire domain of the Indian subcontinent reveals that the daily ISMR range is low (0–400 mm day^{-1}) from the Raw-GEFSv12 day-1 forecast as compared to IMDAA (0–800 mm day^{-1}) (figure not provided). The range of daily ISMR from GEFSv12 is decreasing with lead time, and the upper limit for the lead day 15 is less than 200 mm day^{-1}. After calibration, the daily ISMR rainfall range remarkably improved for all lead times and strengthened the linear relationship (correlation coefficient) with observations. At a grid point from a wet region, the daily ISMR range is much lower (0–50 mm day^{-1}) from the Raw-GEFSv12 than IMDAA (0–500 mm day^{-1}). After calibration, the range of daily ISMR at a wet region for all forecast lead times improved conspicuously. However, the linear relationship with IMDAA decreased substantially. This calibration method has improved the mean climatological features, climatological mean, interannual variability, and CV. But the correlation coefficient may not improve. The reason is that the Q–Q mapping is matching the forecast probability distributions to observations. The success of quantile mapping

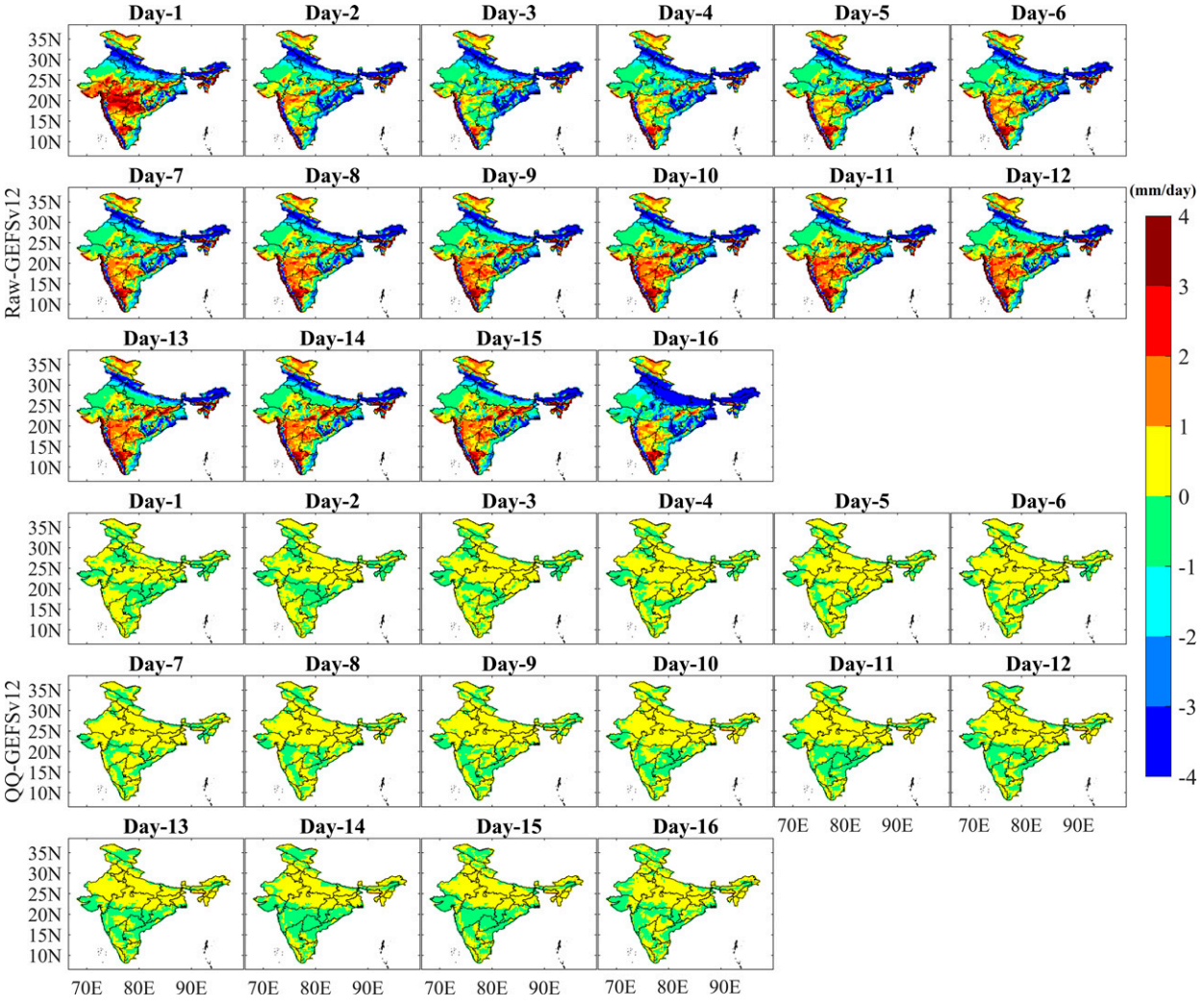

FIG. 2. Mean bias of (a) Raw-GEFSv12 and (b) QQ-GEFSv12 with day-1–16 forecast lead times against IMDAA for JJAS daily rainfall (mm) over Indian subcontinent for the period 2000–19.

also depends on the implicit assumption that the bias in the data is a monotonic transform from the "true" observations. To the extent of other, i.e., nonmonotonic, biases, quantile mapping will not be effective and can even degrade the data. Underlying quantile mapping is the assumption that precipitation bias is primarily related to amount, rather than conditional upon other factors such as the synoptic situation, or other potential predictors such as total column precipitable water. For a dry region, most of the days from the Raw-GEFSv12 are very light to medium-intensity rainfall events. After calibration, the rainfall intensity distribution adjusted well with IMDAA. For better understanding, the daily rainfall plot for the same three cases full domain and wet and dry regions is plotted with a log–log scale and depicted in Fig. 4. After calibration, the improvement in the data range is clearly reflected in all three cases.

We also extended the study with diurnal precipitation analysis and the results demonstrated that the GEFSv12 is able to capture the diurnal variability of Indian monsoon rainfall (figure not provided). It is observed that there is clearly a diurnal cycle from 1800–0000 UTC (high) to 0600–1200 UTC (low) from both Raw and QQ-GEFSv12. However, the Raw-GEFSv12 is a limitation to capture the magnitudes. But the quantile mapping technique could handle this diurnal variability.

The climatological mean pattern of ISMR over India from the Raw-GEFSv12 with day-1, day-5, day-10, and day-15 forecast lead times are similar to IMDAA (Fig. 5). The ISMR is prominent over Western Ghats regions Kerala, Goa, and Coastal Maharashtra, northeast India parts Assam, Meghalaya, Arunachal Pradesh, Nagaland, Manipur, Mizoram, Tripura, and Sikkim, Indo-Gangetic plains Uttarakhand, Uttar Pradesh, and monsoon core regions such as West Bengal, Chhattisgarh, Jharkhand, and Bihar, captured well by the Raw-GEFSv2 for all forecast lead times. The Raw-GEFSv12 is also well represented for the low rainfall zones such as the rainfall shadow region in the south part of south

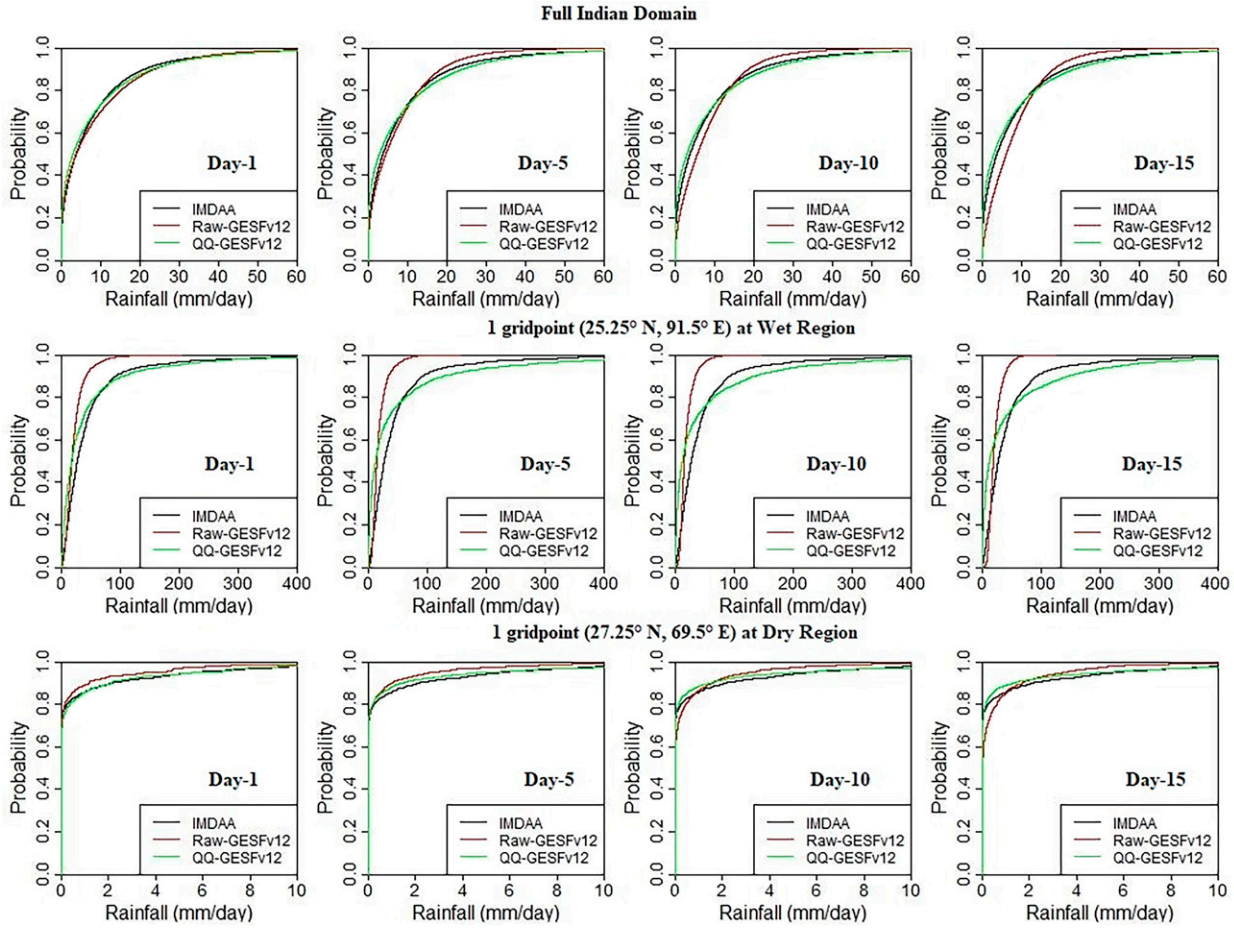

FIG. 3. The day-1, day-5, day-10, and day-15 probability distributions of JJAS 24-h accumulated precipitation for IMDAA (black lines), raw (purple lines), and bias-corrected (green lines) five-member ensemble mean forecasts over the (top) full Indian domain, (middle) wet region, and (bottom) dry region for the period 2000–19.

peninsular India Tamil Nādu, interior parts of Karnataka, southern parts of Andhra Pradesh and Telangana, northwest India parts Gujarat and Rajasthan, and Ladakh regions. Moreover, the day-1 forecasts from Raw-GEFSv12 are relatively closer to the IMDAA than the other forecast lead times. However, the Raw-GEFSv12 for all forecast lead times has a dry bias over prominent rainfall regions, particularly in northeast India, Western Ghats, and monsoon core regions. It also has a wet bias over low rainfall regions, i.e., Ladakh, northwest India, west-central India, and some parts of south peninsular India. After calibration, the ISMR climatological patterns are consistent for all forecast lead times and are similar to IMDAA. The dry bias over prominent rainfall regions and wet bias over low rainfall zones in ISMR for all forecast lead times reduced significantly.

The spatial patterns of interannual variability (IAV; the standard deviation of daily data with respect to the climatological mean precipitation amount) of ISMR over India from the Raw and QQ-GEFSv12 for all forecast lead times are similar to IMDAA (Fig. 6). The IAV of ISMR is maximum over the prominent rainfall regions such as Western Ghats, northeast India, foothills of Himalayan, and monsoon core regions from Raw and QQ-GEFSv12 for all forecast lead times as depicted in IMDAA. The IAV of ISMR from Raw-GEFSv12 day-1 forecast lead times is relatively closer to IMDAA than other forecast lead times where a relatively low bias can be seen. After calibration, the patterns of IAV of ISMR and its magnitude from QQ-GEFSv12 for all the forecast lead times were substantially enhanced and are consistent for all forecast lead times. The box plot analysis reveals that the ISMR spread from Raw-GEFSv12 for day 1 is higher than the IMDAA (Fig. 7a); however, it is much less for day-5, day-10 and day-15 forecast lead times. After calibration, the spread of all forecast lead time is similar to IMDAA, and the median values are also very close to IMDAA (Fig. 7a). In the case of IAV and coefficient of variation (CV; the ratio between standard deviation and climatological mean) analysis from the box plots, the spread of IAV and CV of ISMR from Raw-GEFSv12 for all forecast lead times is remarkably lower than IMDAA (Figs. 7b,c) except for day-1 forecast lead time whereas the overestimation for IAV and CV. The spread of climatological mean, IAV, and CV from Raw-GEFSv12

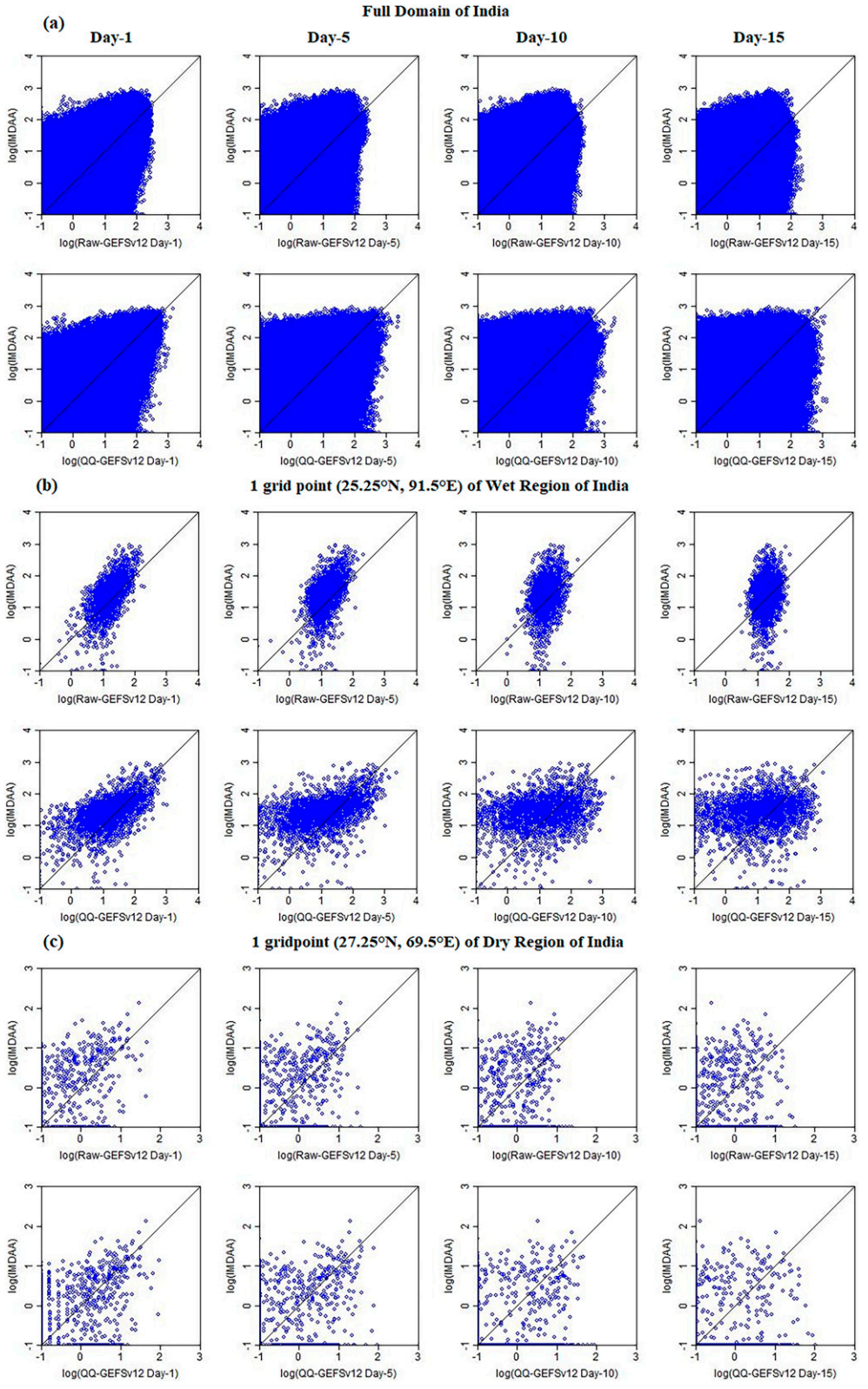

FIG. 4. Log–log scale scatterplot of Raw and QQ-GEFSv12 with day-1, day-5, day-10, and day-15 lead times JJAS daily rainfall forecasts against IMDAA for (a) pooling of all grid points of Indian subcontinent, (b) one grid point at wet region, and (c) one grid point at dry region for ISMR daily rainfall (mm) for the period 2000–19.

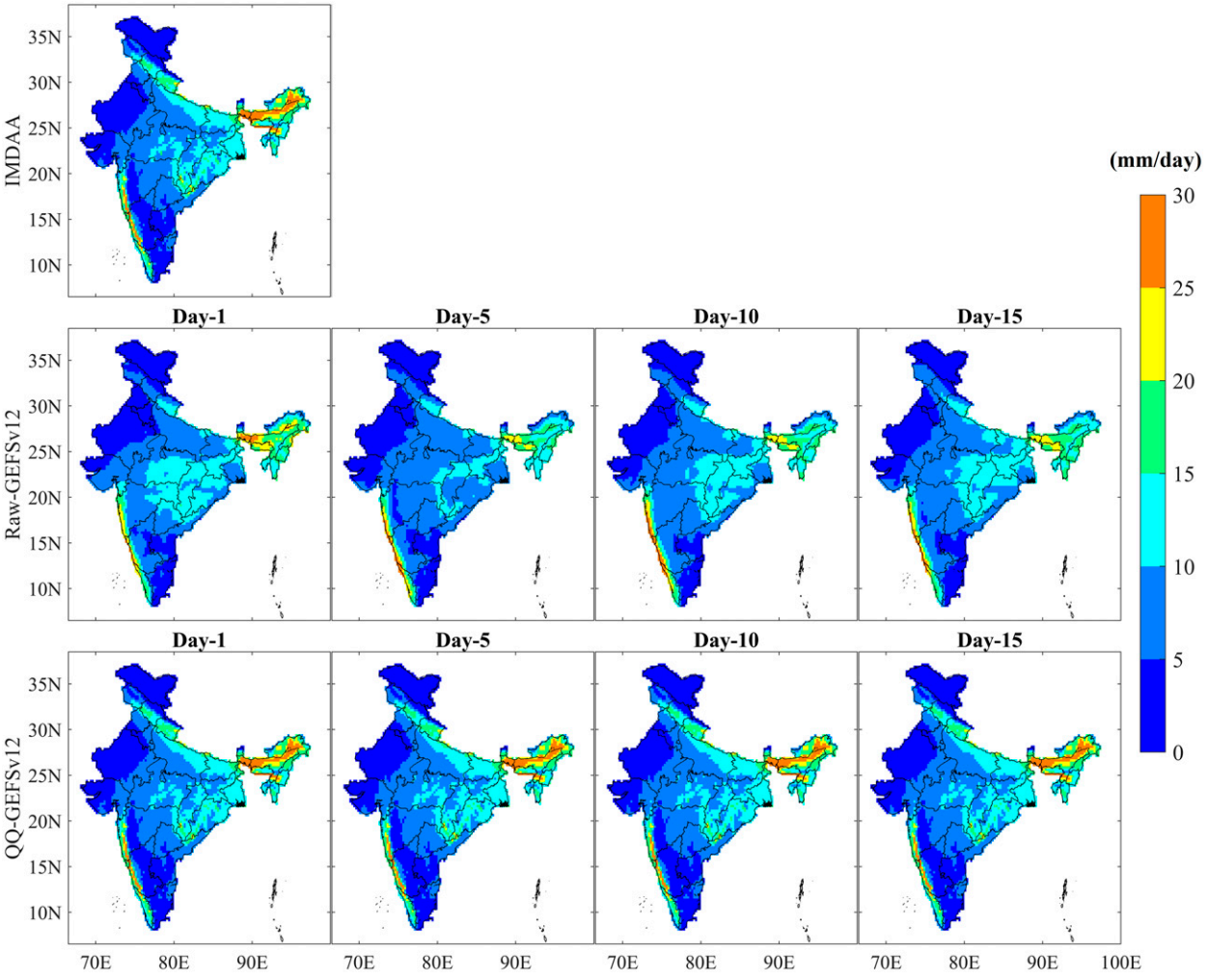

FIG. 5. Spatial distribution of ISMR rainfall from IMDAA and GFSv12 raw and bias-corrected forecasts (with day-1, day-5, day-10, and day-15 lead times) average of JJAS for the period 2000–19.

gradually decreased with lead time. But after calibration, all these features are consistently closer to IMDAA.

The analysis of various categorical rainfall events reveals that the spatial distribution patterns of wet days (>2.5 mm day^{-1}) over India from Raw and calibrated forecasts (QQ-GEFSv12) for all lead times are similar to IMDAA (Fig. 8a). The frequency of wet days is more in prominent ISMR regions such as Western Ghats, northeast India, foothills of Himalaya, and monsoon core regions from Raw and calibrated all forecast lead times. At the same time, the frequency of wet days is relatively less over low rainfall zones such as Ladakh, northwest India, and the shadow region of south peninsular India from Raw and calibrated forecasts (Fig. 8a). The overestimation of wet days by Raw-GEFSv12 over most parts of the country increases with lead time. After calibration, the overestimation of wet days for all forecast lead time is notably reduced (Fig. 8a). The spatial pattern of high-intensity rainfall events (>35.6 mm day^{-1}; RHR to EHR) from Raw-GEFSv12 at all lead times (day 1, 5, 10, 15) forecasts are similar to IMDAA (Fig. 8b); however, there is a substantial underestimation for all forecast lead times except for the day-1 forecast lead time. The underestimation of high-intensity rainfall events from Raw-GEFSv12 gradually increases with lead time, and it is hard to depict high-intensity rainfall events for lead times beyond day 1 (Fig. 8b). The overestimation of ISMR and associated wet days from Raw-GEFSv12 increases with a lead time (Fig. 8a). In contrast, the underestimation of high-intensity rainfall events from Raw-GEFSv12 increases with lead time (Fig. 8b). After calibration, the underestimation of high-intensity rainfall events has substantially improved, resulting in an enhancement in predictability (Fig. 8b). The reduction (enhancement) of wet days (high-intensity rainfall events) during JJAS for day 1, 5, 10, and 15 after calibration is significant at 90% confidence level in most parts of India (Fig. S4). Therefore, the calibrated forecast for high-intensity rainfall events on an extended range scale at the regional level is essential for improving the forecast skill and its application for disaster management planning and managing the risks in agriculture, hydrology, and water resources sectors.

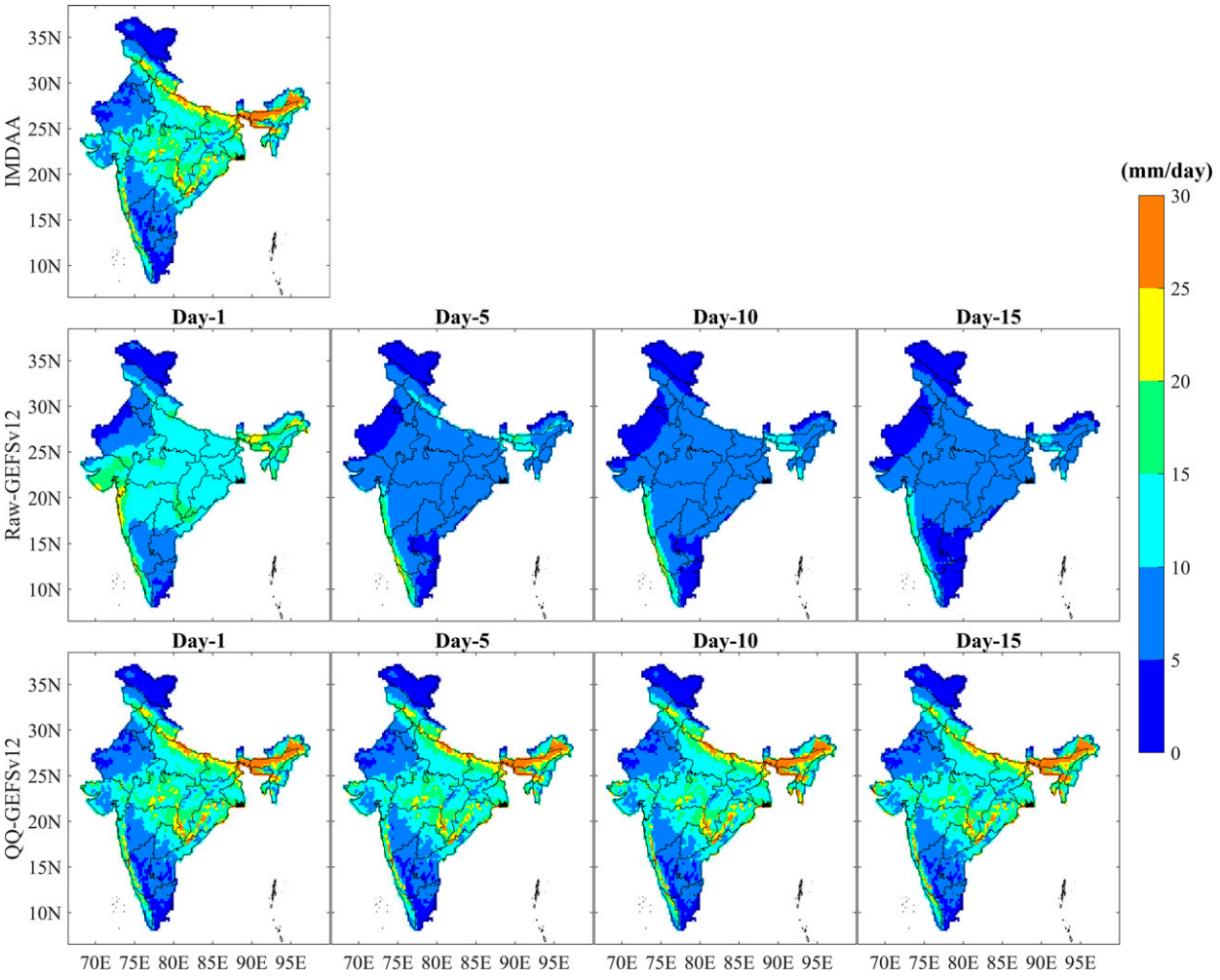

FIG. 6. Spatial distribution of interannual variability of ISMR rainfall (JJAS) from IMDAA and GEFSv12 raw and bias-corrected forecasts (with day-1, day-5, day-10, and day-15 lead times) for the period 2000–19.

The box plot analysis in Fig. 9 reveals that the spread of dry days (wet days) from Raw-GEFSv12 for all forecast lead times is remarkably lower (higher) than the IMDAA except for the day-1 forecast lead time. The underestimation of dry days from Raw-GEFSv12 increases gradually with lead time, while the overestimation of wet days from Raw-GEFSv12 increases gradually with lead time. After calibration, the number of wet days (dry days) is notably reduced (increased) for all forecast lead times by adjusting the rainfall intensity probability distributions of the model to IMDAA. There is an underestimation of VLR days from Raw-GEFSv12 for all forecast lead times, which increased gradually with the lead time. After calibration, the estimation of VLR days outstandingly improved. There is an overestimation of LR and MR from Raw-GEFSv12 for all forecast lead times except for the day-1 forecast lead time for LR. After calibration, MR events distribution from QQ-GEFSv12 is relatively closer to IMDAA than the Raw-GEFSv12, while a substantial underestimation has been found for LR events. A considerable underestimation was found for high-intensity rainfall events (>35.6 mm day^{-1}; RHR, HR, VHR, and EHR events) from Raw-GEFSv12 for all forecast lead times. There are no VHR and EHR events from Raw-GEFSv12. After calibration, the spread of high-intensity rainfall events for RHR, HR, VHR, and EHR events from QQ-GEFSv12 adjusted well with IMDAA.

Further, various statistical categorical skill scores (such as POD, frequency bias, ACC, SR, TS, and ETS, etc.) by using the contingency table have been computed for various rainfall events from raw and calibrated (QQ-GEFSv12) for day-1, day-5, day-10, and day-15 forecast lead times against IMDAA for the reforecast period 2000–19 and is illustrated in box plots in Figs. 10 and 11 and performance diagrams in Fig. 12. The box plot analysis of frequency bias reveals a considerable underestimation of dry days, VLR, RHR, HR, VHR, and EHR from Raw GEFSv12 for all forecast lead times. In contrast, there is a large overestimation for LR and wet days (Fig. 10). After calibration, the overestimation/underestimation for various rainfall events reduced remarkably (frequency bias is ~1) for all forecast lead times, and the improvement is particularly more for high-intensity rainfall events.

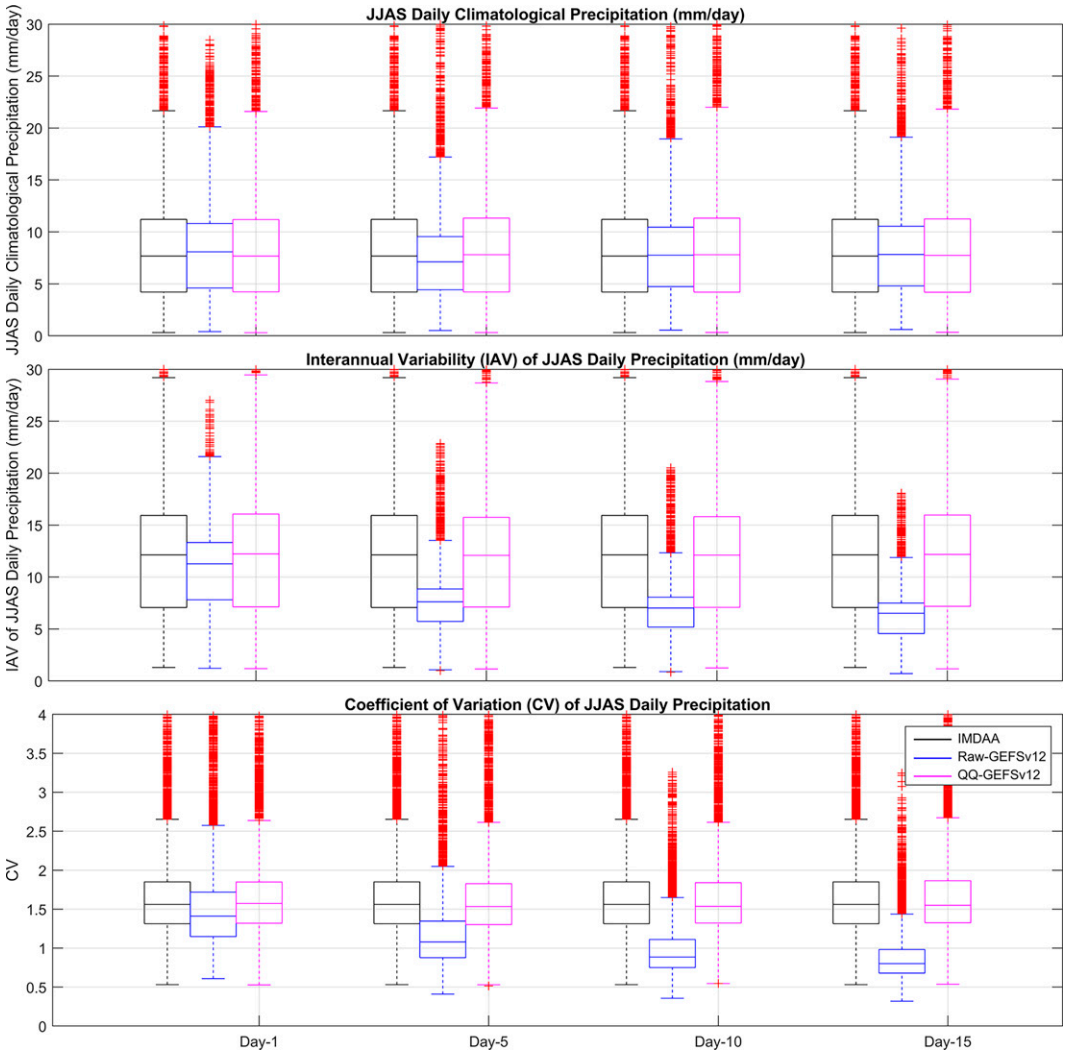

FIG. 7. Boxplot for pooling of all grid points of Indian subcontinent for JJAS daily rainfall (a) climatological mean; (b) interannual variability; and (c) coefficient of variation from IMDAA, Raw, and QQ-GEFSv12 for day 1, 5, 10, and 15 for the period 2000–19. The black, blue, and magenta boxes represent the IMDAA, Raw, and QQ-GEFSv12, respectively; while the top and bottom lines of the boxes represent the 75th and the 25th percentiles, respectively. The middle line in the box represents the median, and the vertical line extends from the 1st to 99th percentiles. The red color indicates the outliers of the data (>99th percentile data).

The accuracy of various intensity rainfall events from Raw and QQ-GEFSv12 is decreasing with lead time (Fig. S5). However, the accuracy for high-intensity rainfall events (>35.6 mm day^{-1}; RHR, HR, VHR, and EHR) is >0.9 for all forecast lead times from Raw and QQ-GEFSv12. After calibration, the accuracy of LR, MR, RHR, HR, VHR, and EHR is marginally improved for all forecast lead times. The improvement is mainly due to the rainfall intensity probability adjustment from model to observations. After calibration, there is a notable improvement in ETS score for dry days, wet days, LR, MR, RHR, HR, VHR, and EHR in all forecast lead times, while slight decreases in ETS for VLR events (Fig. 11). A performance diagram is one method to present several categorical skill scores such as POD, BIAS, TS, and SR (1-FAR) together on a single diagram (Fig. 12). The performance diagram for wet days (>2.5 mm day^{-1}) indicates that the Raw-GEFSv12 has a considerable overestimation of wet days for all forecast lead times, and it increases with lead time (Fig. 12a). After calibration, the overestimation of wet days reduces substantially for all forecast lead times while the POD of wet days for all lead times has decreased. It is interesting to notice that the POD for wet days from Raw-GEFSv12 (QQ-GEFSv12) is more for long (shorter) lead times than the short (longer) lead-time forecasts. The large overestimation of wet days, as well as low-to-moderate-intensity rainfall events from Raw-GEFSv12, is led to high skill scores of POD for wet days and low-to-moderate intensity rainfall events. The calibration method significantly reduced the overestimation of wet and low-to-moderate-intensity rainfall events and caused a decrease in

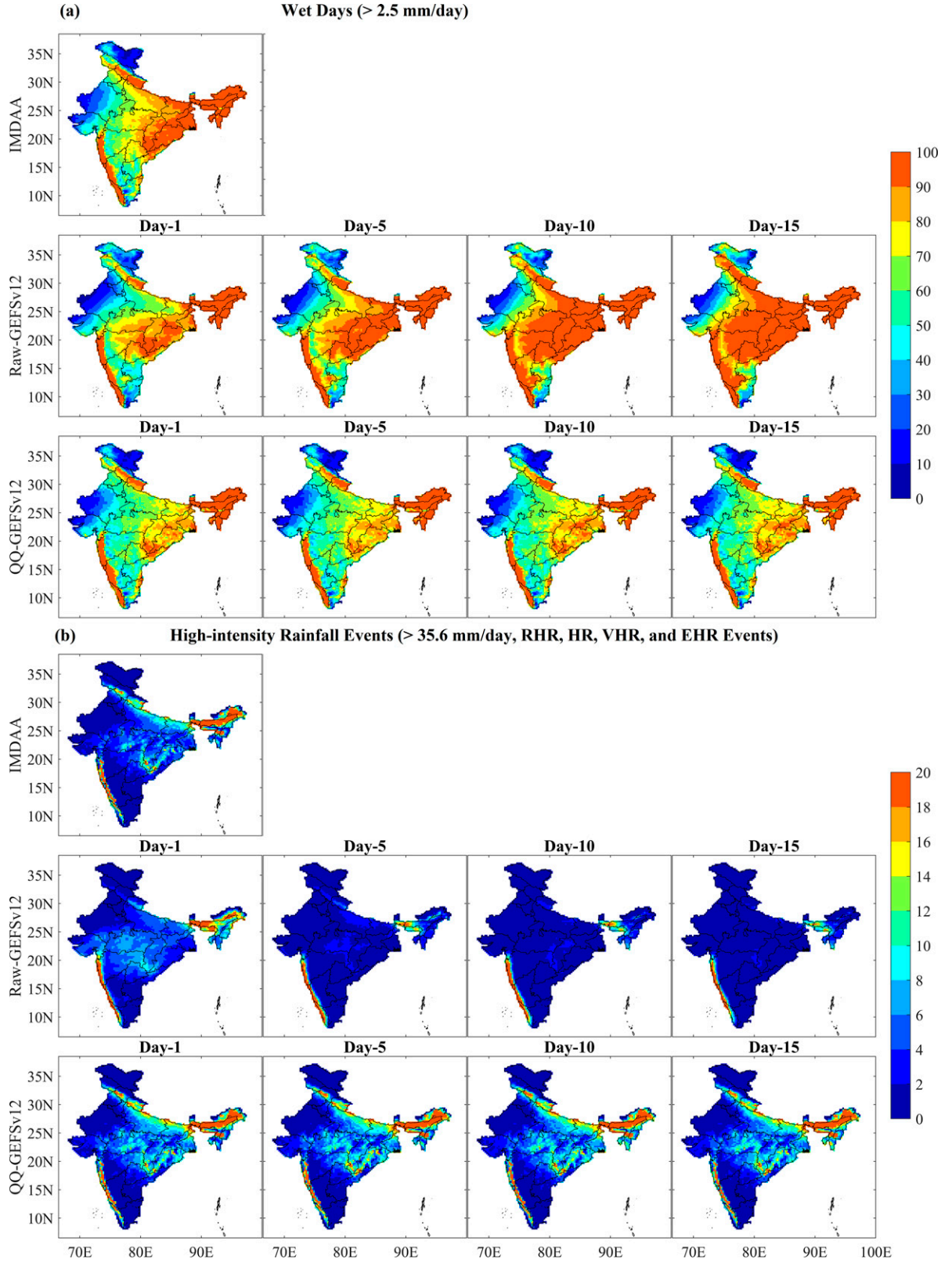

FIG. 8. Spatial distribution of (a) wet days and (b) high-intensity rainfall events during JJAS over India from IMDAA, Raw, and QQ-GEFSv12 (with day-1, day-5, day-10, and day-15 lead times) for the period 2000–19.

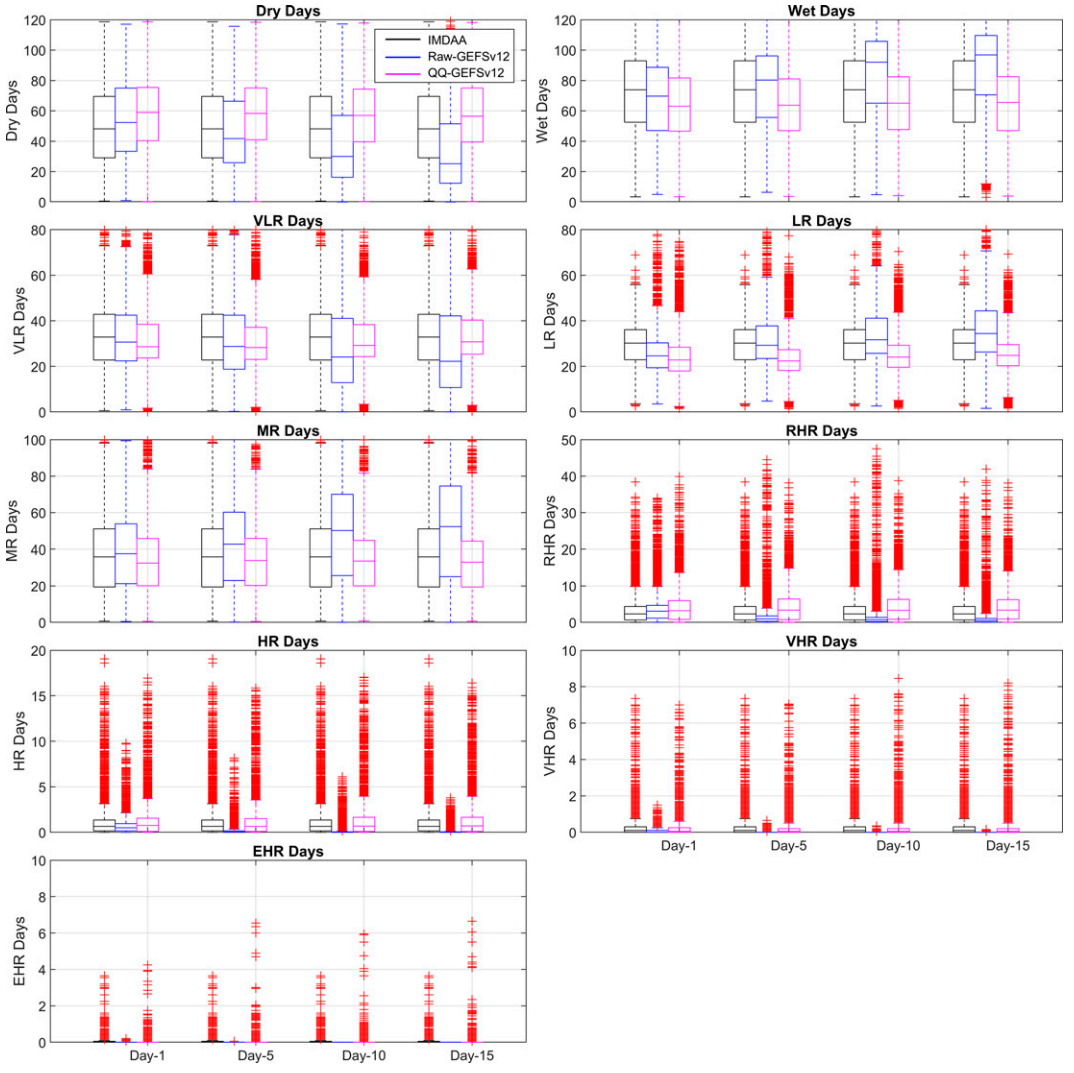

FIG. 9. Boxplot for pooling of Indian domain all grid point's various categorical rainfall events (such as dry days, wet days, VLR, LR, MR, RHR, HR, VHR, and EHR events) during JJAS from IMDAA, Raw, and QQ-GEFSv12 for day-1, day-5, day-10, and day-15 lead times for the period 2000–19. The black, blue, and magenta boxes represent the IMDAA, Raw, and QQ-GEFSv12, respectively; while the top and bottom lines of the boxes represent the 75th and the 25th percentiles, respectively. The middle line in the box represents the median, and the vertical line extends from the 1st to 99th percentiles. The red color indicates the outliers of the data (>99th percentile data).

the POD skill score (Figs. 12a,b). The TS and SR skill scores for wet days from Raw and QQ-GEFSv12 also increase with lead time. Most of the skill scores of low-to-medium intensity rainfall events (2.5–35.5 mm day^{-1}) are similar to wet days (Fig. 12b). After calibration, there is a remarkable increase in most skill scores for high-intensity rainfall events for all forecast lead times (Fig. 12c). Jiang et al. (2017) has also found the overestimation (underestimation) of low-to-medium-intensity rainfall events (heavy- to extremely heavy–intensity rainfall events) over the tropics from the GEFS model and particularly more during the summer monsoon season. It is well known that the aerosol–cloud interactions and aerosol–radiation interactions play a vital role in precipitation occurrences with different intensity levels over various parts of the globe (Twomey et al. 1984; Albrecht 1989; Rosenfeld et al. 2008; Tao et al. 2012). Along with many other factors, the model's inability to represent aerosol effects on precipitation, i.e., the inhibition of light rain and the enhancement of heavy rain by aerosols in the model is one of the possible reasons to account for these biases for various intensity rainfall events (Jiang et al. 2017).

The deterministic methods cannot represent the inherent uncertainty in forecasts if the uncertainty estimated for the particular category forecast is more helpful, especially for the climate risk management in various sectors. Nowadays, probabilistic forecasts are vital for weather and climate extremes at various time scales (Mason and Graham 1999; Palmer et al. 2004; Mason 2004). The performance evaluation has been extended to the probabilistic forecast for wet (>2.5 mm day^{-1}) and ER

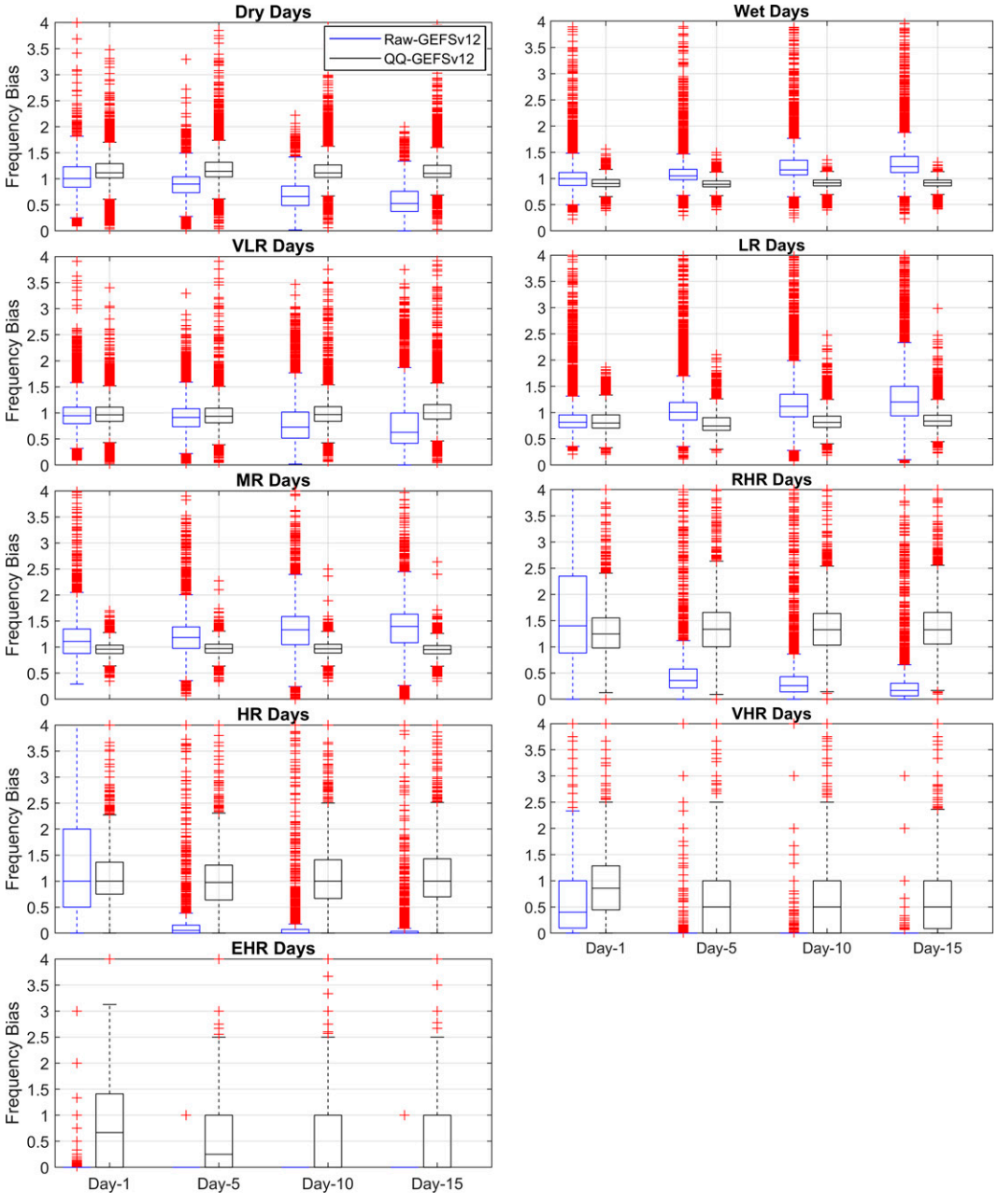

FIG. 10. Boxplot for BIAS (frequency bias) of Raw and QQ-GEFSv12 with day-1, day-5, day-10, and day-15 lead times against IMDAA for various categorical JJAS daily rainfall events such as dry days, wet days, VLR, LR, MR, RHR, HR, VHR, and EHR events of all grid points of Indian subcontinent for the period 2000–19. The blue and black boxes represent the Raw and QQ-GEFSv12, respectively; while the top and bottom lines of the boxes represent the 75th and the 25th percentiles, respectively. The middle line in the box represents the median, and the vertical line extends from the 1st to 99th percentiles. The red color indicates the outliers of the data (>99th percentile data).

(>35.6 mm day^{-1}; RHR, HR, VHR, and VHR) events by using standard probabilistic forecast skill metrics such as reliability, resolution, Brier score, and ranked probabilistic score (Brier 1950; Epstein 1969; Murphy 1993; Toth et al. 2003; Mason 2004; Wilks 2011). The probabilistic skill scores analysis reveals that most of the probabilistic skill scores of wet and ER events decrease with lead time from Raw and QQ-GEFSv12 (Fig. 13). The marginal improvement for all the probabilistic skill scores for both wet and ER Events is noticed after calibration.

4. Summary and conclusions

Extreme rainfall events (ER) are responsible for floods and cause widespread destruction of infrastructure, economic

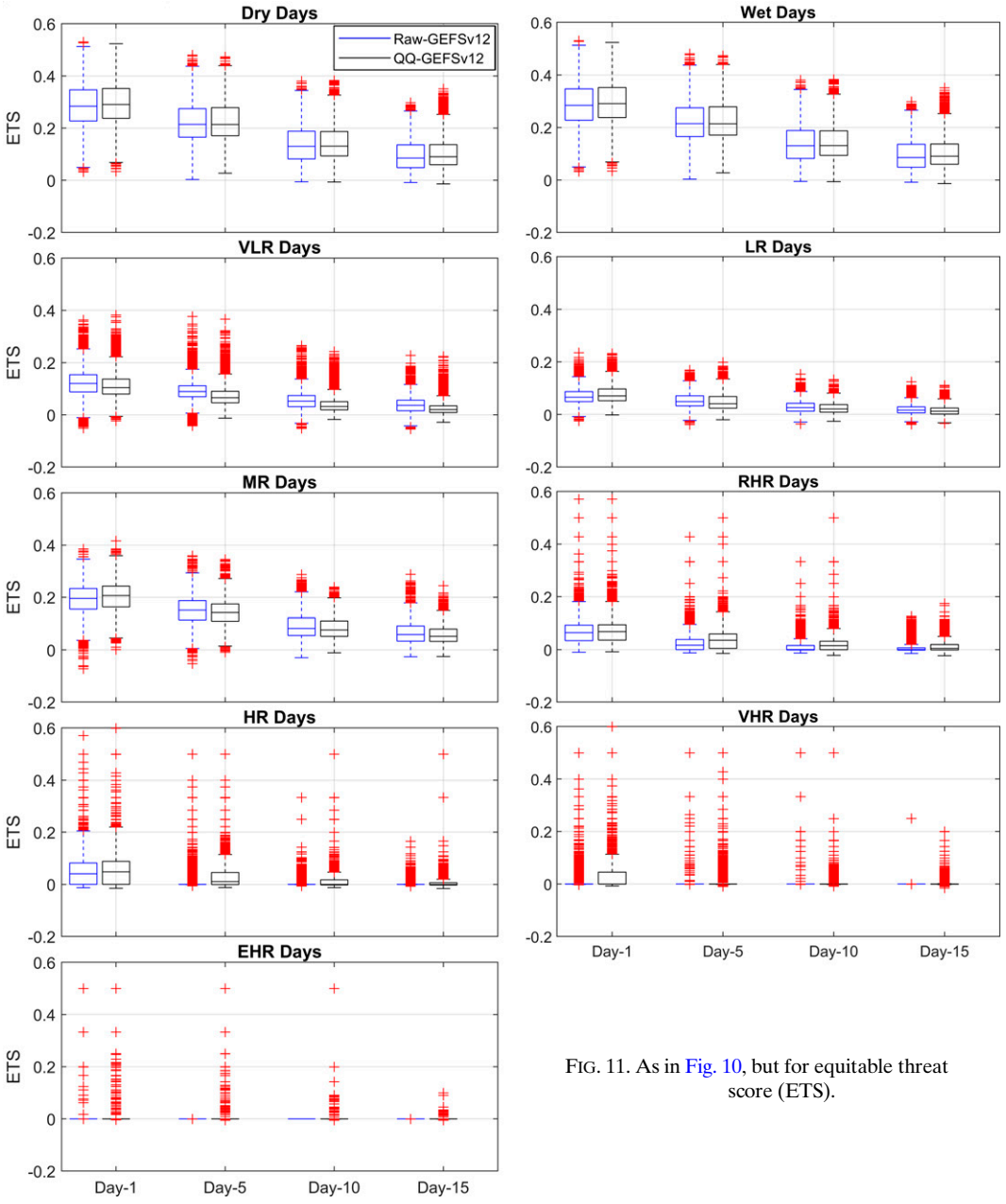

FIG. 11. As in Fig. 10, but for equitable threat score (ETS).

damage, and the loss of lives, causing a monetary loss. It is also evident that the frequency of ER and prolonged droughts outstandingly increased in recent decades in various parts of India. It is mainly during the Indian summer monsoon (ISM) season (JJAS), which contributes 80% of the annual total rainfall in this region. This season is the primary cropping season in India. The variations in crop production are mainly due to the variability in weather and climate on various time scales such as short, medium, extended, and seasonal scales over this region. The prediction skill of the numerical models is at a satisfactory level up to day-5 forecasts and seasonal outlooks in most parts of the globe, and it is notably higher for extratropical regions than the tropics and monsoon regions. The extended range forecast skill (from beyond 10 days to 1 month) is considerably low and is one of the most challenging tasks for the meteorological community. The low skill of this time scale is mainly because much of the memory of the initial atmospheric conditions on this time scale range is lost. Imperfect forecast model systems could not catch up with the atmosphere's nonlinearity and chaos, affecting the prediction skill. On the other hand, the subseasonal (weeks 2–4) scales are not large enough for the atmospheric signal associated with the ocean anomalies to emerge over the atmospheric noise. Improved forecasts of Indian summer monsoon rainfall (ISMR) and associated extreme

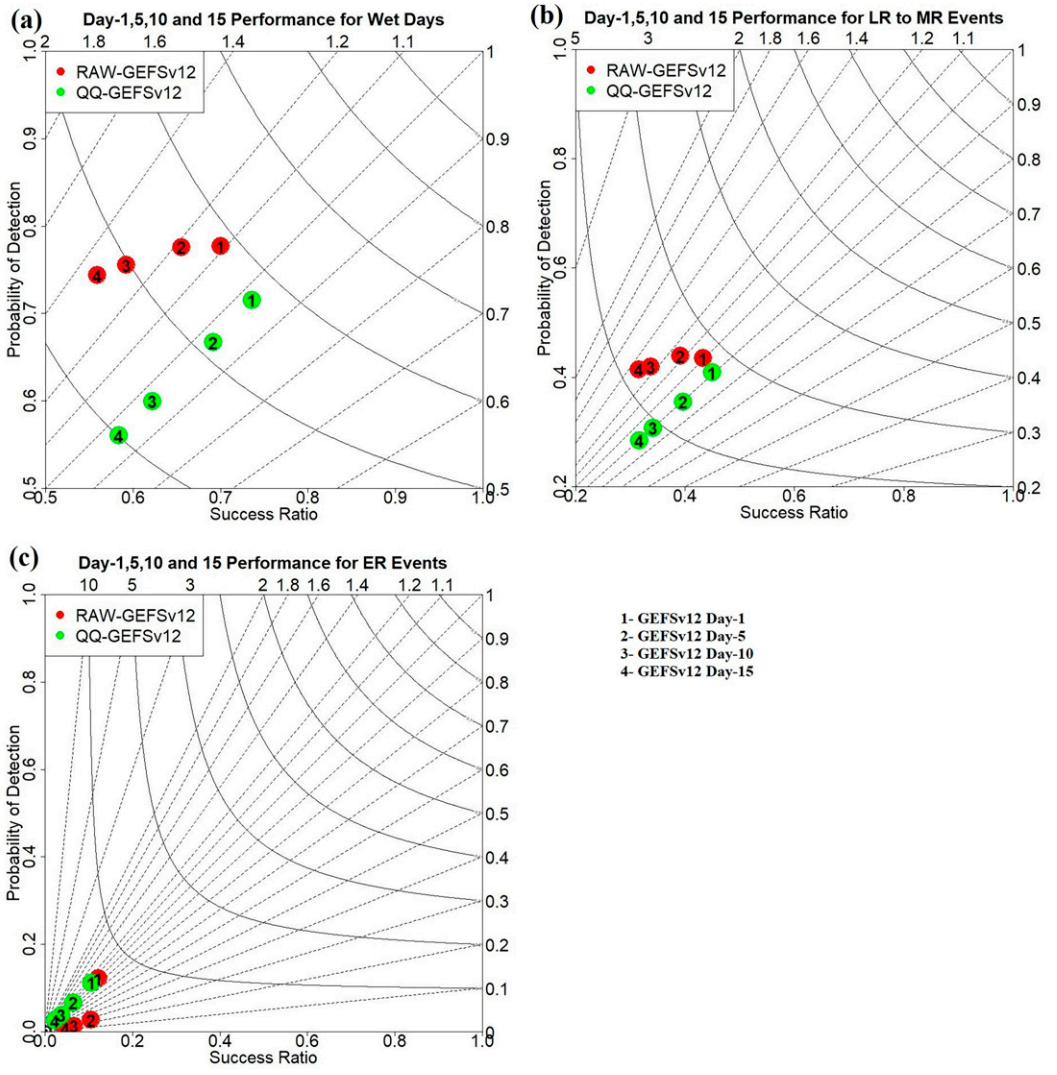

FIG. 12. Performance diagram summarizing the SR, POD, frequency bias, and TS statistical categorical skill scores of Raw and QQ-GEFSv12 with day-1–16 forecast lead times against IMDAA for (a) wet days, (b) low- to medium-intensity rainfall events, and (c) high- to extreme-intensity rainfall events over India during JJAS for the period 2000–19. The solid contour lines in the performance diagram show the TS, while the dashed lines show the frequency bias with extended labels on the *x* and *y* upper (second) axes.

rainfall events on an extended range time scale over the Indian subcontinent are in high demand by various risk management sectors. The present study evaluated the NCEP GEFSv12 in depicting ISMR and extreme rainfall events over the Indian subcontinent on an extended range time scale against the IMDAA (2000–19). A quantile mapping calibration technique is applied to enhance the prediction skill of GEFSv12 rainfall reforecast products.

The results of the present study suggest that the GEFSv12 is able to capture the diurnal variability of Indian monsoon rainfall. It is observed that there is clearly a diurnal cycle from 1800–0000 UTC (high) to 0600–1200 UTC (low) from both Raw and QQ-GEFSv12. However, the Raw-GEFSv12 is a limitation to capture the magnitudes. But, the quantile mapping technique could handle this diurnal variability. The ISMR patterns from Raw-GEFSv12 with (lead) day 1–16 are similar to the IMDAA reanalysis. However, Raw-GEFSv12 has a large dry bias in prominent ISMR regions, including the monsoon core zone, northeast India, Western Ghats, and Foothills of Himalayan for all forecast lead times (day 1–16) while a wet bias over low ISMR regions rainfall shadow exists in the region of south peninsular India, Ladakh, west-central and northwest parts of India for all forecast lead times. Various intensity rainfall events' analysis indicates that in most parts of the country, the total number of wet days is remarkably more in Raw-GEFSv12 than in IMDAA. The frequency of the low- and medium-intensity rainfall events (LR and MR) from Raw-GEFSv12 is remarkably higher than that

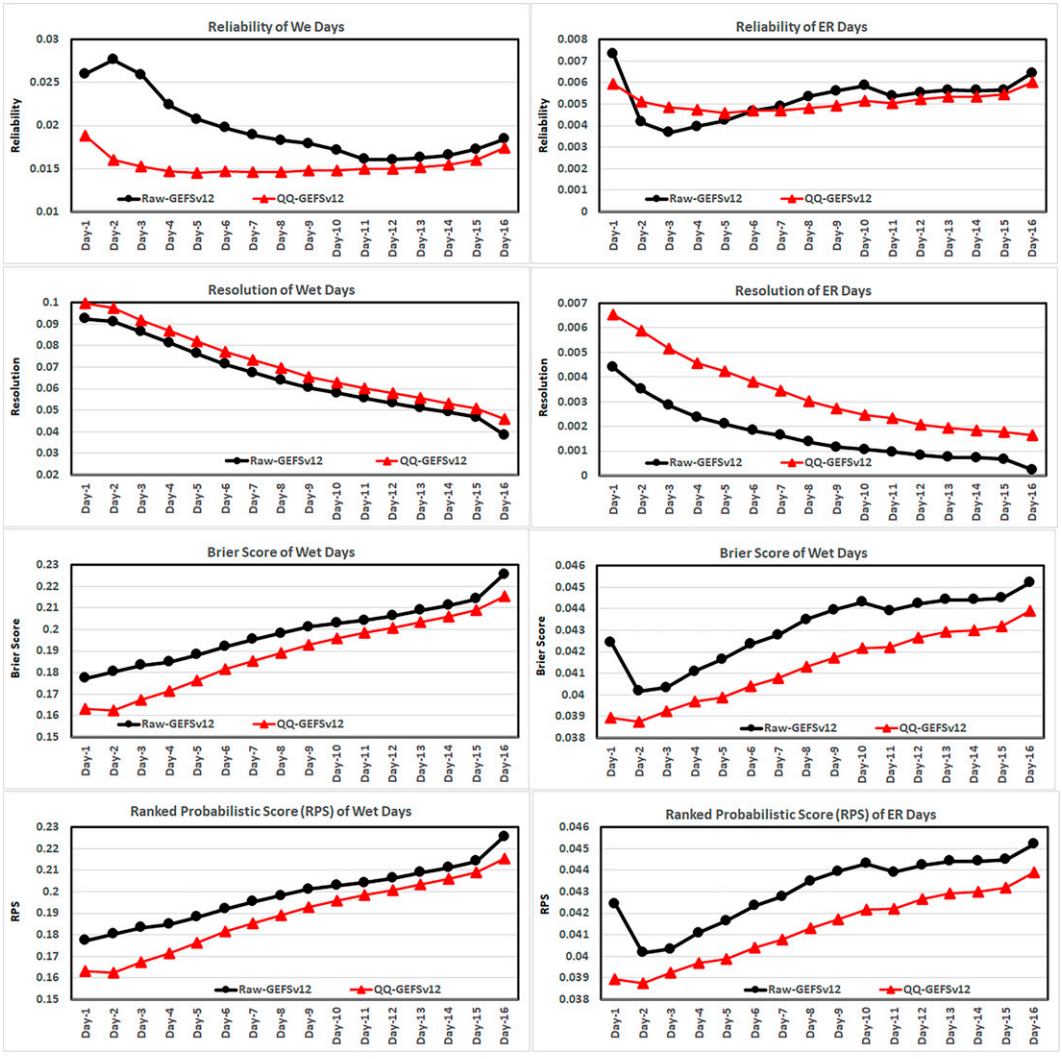

FIG. 13. (row 1) Reliability, (row 2) resolution, (row 3) Brier score, and (row 4) ranked probabilistic score of (left) wet and (right) ER events' probabilistic forecast over India during southwest summer monsoon (June–September) from Raw and QQ-GEFSv12 against IMDAA for forecast lead time day-1–16 for the period 2000–19.

from IMDAA. In contrast, high- to extremely high–intensity rainfall events (RHR, HR VHR, and EHR) are remarkably less in Raw-GEFSv12. The prediction skill of Raw-GEFSv12 decreased remarkably with lead lime (day 1–16). It is interesting to notice that after calibration, the prediction skill for all forecast lead times is consistent with marginal improvement. The calibration method also marginally improved most of the statistical categorical skill scores (BIAS, ACC, SR, FAR, and POD) of various intensity rainfall events and was consistent for all forecast lead times. The improvement is particularly more for high to extreme-intensity rainfall events (>35.6 mm day^{-1}). The calibration method improves the probability distribution of various intensity rainfall events from model to observation for all forecast lead times (day 1–16). The probabilistic skill scores analysis reveals that most of the probabilistic skill scores (reliability, resolution, Brier score, and ranked probabilistic score) of wet and ER events decrease with lead time from Raw and QQ-GEFSv12. The marginal improvement in probabilistic skill scores for both wet and ER events is noticed after calibration. The calibration of precipitation forecasts is essential to enhance forecast skill on an extended range time scale to increase usability in various risk management sectors.

Therefore, the calibration of GEFSv12 model rainfall products using the quantile mapping postprocessing technique is a useful tool to provide the rainfall forecast guidance over India on the extended range time scale, along with short and medium-range, which can be helpful for tactical adjustments to the strategic decisions made based on the long-lead seasonal forecast outlooks for managing the risk in various sectors due to floods and droughts at a regional level.

Future scope

The present performance evaluation of GEFSv12 rainfall reforecast over India will be extended to sub-seasonal/

monthly scales by using every Wednesday 0000 UTC initial conditions with 11 ensemble members. The calibration method will be applied for all individual members to improve the prediction skill of probabilistic forecasts, which will help understand the forecast uncertainty for proper decision-making. We also proposed a neural network (NN)-based calibration method that can incorporate nonlinear relationships between arbitrary predictor variables and forecast distribution parameters that are automatically learned in a data-driven way rather than requiring pre-specified link functions. This method will be compared with other traditional statistical post-processing methods.

Acknowledgments. This work is carried out with generous funding support from the NCEP Visiting Scientist Program managed by the University Corporation for Atmospheric Research (UCAR) Cooperative Programs for the Advancement of Earth System Science (CPAESS). The authors are grateful to the Ensemble Team members at the NCEP Environmental Modeling Center (EMC) and National Center for Medium-Range Weather Forecasts (NCMRWF), India, for providing access to the datasets used in this study. Drs. Partha Bhattacharjee, Eric Sinsky, and Mary Hart are thanked for their careful reviews of the manuscript. The authors are also very appreciative of the anonymous reviewers for providing valuable suggestions and comments that were helpful for the improvement of the quality of the manuscript.

Data availability statement. The GEFSv12 precipitation reforecast products over the Indian subcontinent for the reforecast period (2000–19) have been obtained from Amazon Web Services (AWS; https://noaa-gefs-retrospective.s3.amazonaws.com/index.html), which are accessible by the broader community. The Indian Monsoon Data Assimilation and Analysis (IMDAA) used as reference dataset that is freely available at Data Web portal (https://rds.ncmrwf.gov.in/dashboard/download) of National Center for Medium-Range Forecasting (NCMRWF), Earth System Science Organization, Ministry of Earth Sciences, government of India. The India Meteorological Department (IMD) gridded observed analysis rainfall dataset with 0.25° × 0.25° horizontal resolution is available at https://imdpune.gov.in/Clim_Pred_LRF_New/Grided_Data_Download.html. The CMORPH daily rainfall data with 0.25° × 0.25° horizontal resolution is accessible from https://www.ncei.noaa.gov/data/cmorph-high-resolution-global-precipitation-estimates/access/daily/0.25deg/.

REFERENCES

Abhik, S., R. P. M. Krishna, M. Mahakur, M. Ganai, P. Mukhopadhyay, and J. Dudhia, 2017: Revised cloud processes to improve the mean and intraseasonal variability of Indian summer monsoon in climate forecast system: Part 1. *J. Adv. Model. Earth Syst.*, **9**, 1002–1029, https://doi.org/10.1002/2016MS000819.

Abhilash, S., A. K. Sahai, S. Pattnaik, B. N. Goswami, and A. Kumar, 2013a: Extended range prediction of active-break spells of Indian summer monsoon rainfall using an ensemble prediction system in NCEP climate forecast system. *Int. J. Climatol.*, **34**, 98–113, https://doi.org/10.1002/joc.3668.

——, ——, N. Borah, R. Chattopadhyay, S. Joseph, S. Sharmila, S. De, and B. N. Goswami, 2013b: Does bias correction in the forecasted SST improve the extended range prediction skill of active-break spells of Indian summer monsoon rainfall? *Atmos. Sci. Lett.*, **15**, 114–119, https://doi.org/10.1002/asl2.477.

——, ——, ——, ——, ——, ——, ——, and ——, 2014: Prediction and monitoring of monsoon intra-seasonal oscillations over Indian monsoon region in an ensemble prediction system using CFSv2. *Climate Dyn.*, **42**, 2801–2815, https://doi.org/10.1007/s00382-013-2045-9.

Adhikari, P., Y. Hong, K. R. Dougla, D. B. Kirschbaum, J. Gourley, R. Adler, and G. R. Brakenridge, 2010: A digitized global flood inventory (1998–2008): Compilation and preliminary results. *Nat. Hazards*, **55**, 405–422, https://doi.org/10.1007/s11069-010-9537-2

Ahasan, M. N., M. A. M. Chowdhury, and D. A. Quadir, 2013: Simulation of high impact rainfall events over southeastern hilly region of Bangladesh using MM5 model. *Int. J. Atmos. Sci.*, **2013**, 657108, https://doi.org/10.1155/2013/657108

Albrecht, B. A., 1989: Aerosols, cloud microphysics, and fractional cloudiness. *Science*, **245**, 1227–1230, https://doi.org/10.1126/science.245.4923.1227.

Alpert, J. C., M. Kanamitsu, P. M. Caplan, J. G. Sela, G. H. White, and E. Kalnay, 1988: Mountain induced gravity wave drag parameterization in the NMC medium-range forecast model. *Eighth Conf. on Numerical Weather Prediction*, Baltimore, MD, Amer. Meteor. Soc., 726–733.

Ashrit, R., and Coauthors, 2020: IMDAA regional reanalysis: Performance evaluation during Indian summer monsoon season. *J. Geophys. Res. Atmos.*, **125**, e2019JD030973, https://doi.org/10.1029/2019JD030973.

Barde, V., M. M. Nageswararao, U. C. Mohanty, R. K. Panda, and M. Ramadas, 2020: Characteristics of southwest summer monsoon rainfall events over East India. *Theor. Appl. Climatol.*, **141**, 1511–1528, https://doi.org/10.1007/s00704-020-03251-y.

Bauer, P., A. Thorpe, and G. Brunet, 2015: The quiet revolution of numerical weather prediction. *Nature*, **525**, 47–55, https://doi.org/10.1038/nature14956.

Boers, N., B. Bookhagen, H. M. J. Barbosa, N. Marwan, J. Kurths, and J. A. Marengo, 2014: Prediction of extreme floods in the eastern Central Andes based on a complex networks approach. *Nat. Commun.*, **5**, 5199, https://doi.org/10.1038/ncomms6199.

Brier, G. W., 1950: Verification of forecasts expressed in terms of probability. *Mon. Wea. Rev.*, **78**, 1–3, https://doi.org/10.1175/1520-0493(1950)078<0001:VOFEIT>2.0.CO;2.

Buizza, R., M. Miller, and T. Palmer, 1999: Stochastic representation of model uncertainties in the ECMWF Ensemble Prediction System. *Quart. J. Roy. Meteor. Soc.*, **125**, 2887–2908, https://doi.org/10.1002/qj.49712556006.

Chun, H. Y., and J. J. Baik, 1998: Momentum flux by thermally induced internal gravity waves and its approximation for large-scale models. *J. Atmos. Sci.*, **55**, 3299–3310, https://doi.org/10.1175/1520-0469(1998)055<3299:MFBTII>2.0.CO;2.

Clough, S. A., M. W. Shephard, E. J. Mlawer, J. S. Delamere, M. J. Iacono, K. Cady-Pereira, S. Boukabara, and P. D. Brown, 2005: Atmospheric radiative transfer modeling: A summary of the AER codes. *J. Quant. Spectrosc. Radiat.*

Transfer, **91**, 233–244, https://doi.org/10.1016/j.jqsrt.2004.05.058.

Deb, S. K., C. M. Kishtawal, V. S. Bongirwar, and P. K. Pal, 2010: The simulation of heavy rainfall episode over Mumbai: Impact of horizontal resolutions and cumulus parameterization schemes. *Nat. Hazards*, **52**, 117–142, https://doi.org/10.1007/s11069-009-9361-8.

Dube, A., R. Ashrit, A. Ashish, K. Sharma, G. R. Iyengar, E. N. Rajagopal, and S. Basu, 2014: Forecasting the heavy rainfall during Himalayan flooding—June 2013. *Wea. Climate Extremes*, **4**, 22–34, https://doi.org/10.1016/j.wace.2014.03.004.

Ebert, E. E., 2001: Ability of a poor man's ensemble to predict the probability and distribution of precipitation. *Mon. Wea. Rev.*, **129**, 2461–2480, https://doi.org/10.1175/1520-0493(2001)129<2461:AOAPMS>2.0.CO;2.

Endo, N., J. Matsumoto, and T. Lwin, 2009: Trends in precipitation extremes over Southeast Asia. *SOLA*, **5**, 168–171, https://doi.org/10.2151/sola.2009-043.

Epstein, E. S., 1969: A scoring system for probability forecasts of ranked categories. *J. Appl. Meteor.*, **8**, 985–987, https://doi.org/10.1175/1520-0450(1969)008<0985:ASSFPF>2.0.CO;2.

Francis, P. A., and S. Gadgil, 2006: Intense rainfall events over the west coast of India. *Meteor. Atmos. Phys.*, **94**, 27–42, https://doi.org/10.1007/s00703-005-0167-2.

Gadgil, S., 2000: Monsoon-ocean coupling. *Curr. Sci.*, **78**, 309–323.

——, 2003: The Indian monsoon and its variability. *Annu. Rev. Earth Planet. Sci.*, **31**, 429–467, https://doi.org/10.1146/annurev.earth.31.100901.141251.

Ganai, M., P. Mukhopadhyay, R. P. M. Krishna, and M. Mahakur, 2015: The impact of revised, simplified Arakawa–Schubert convection parameterization scheme in CFSv2 on the simulation of the Indian summer monsoon. *Climate Dyn.*, **45**, 881–902, https://doi.org/10.1007/s00382-014-2320-4.

——, R. P. M. Krishna, P. Mukhopadhyay, and M. Mahakur, 2016: The impact of revised, simplified Arakawa–Schubert scheme on the simulation of mean and diurnal variability associated with active and break phases of Indian summer monsoon using CFSv2. *J. Geophys. Res. Atmos.*, **121**, 9301–9323, https://doi.org/10.1002/2016JD025393.

——, P. Mukhopadhyay, R. P. M. Krishna, S. Abhik, and M. Halder, 2019: Revised cloud and convective parameterization in CFSv2 improve the underlying processes for northward propagation of intraseasonal oscillations as proposed by the observation-based study. *Climate Dyn.*, **53**, 2793–2805, https://doi.org/10.1007/s00382-019-04657-9.

George, P. A., 1956: Effects of offshore vortices on rainfall along the west coast of India. *Indian J. Meteor. Geophys.*, **7**, 225–240.

Ghosh, S., V. Luniya, and A. Gupta, 2009: Trend analysis of Indian summer monsoon rainfall at different spatial scales. *Atmos. Sci. Lett.*, **10**, 285–290, https://doi.org/10.1002/asl.235.

Goswami, B. N., and S. Chakravorty, 2017: Dynamics of the Indian summer monsoon climate. *Oxford Research Encyclopedia of Climate Science*, Oxford University Press, https://doi.org/10.1093/acrefore/9780190228620.013.613.

——, V. Venugopal, D. Sengupta, M. S. Madhusoodanan, and P. K. Xavier, 2006: Increasing trend of extreme rain events over India in a warming environment. *Science*, **314**, 1442–1445, https://doi.org/10.1126/science.1132027.

Guan, H., and Coauthors, 2022: GEFSv12 reforecast dataset for supporting subseasonal and hydrometeorological applications. *Mon. Wea. Rev.*, **150**,647–665, https://doi.org/10.1175/MWR-D-21-0245.1.

Guhathakurta, P., O. P. Sreejith, and P. A. Menon, 2011: Impact of climate change on extreme rainfall events and flood risk in India. *J. Earth Syst. Sci.*, **120**, 359–373, https://doi.org/10.1007/s12040-011-0082-5.

Hamill, T. M., and J. S. Whitaker, 2006: Probabilistic quantitative precipitation forecasts based on reforecast analogs: Theory and application. *Mon. Wea. Rev.*, **134**, 3209–3229, https://doi.org/10.1175/MWR3237.1.

——, and Coauthors, 2022: The reanalysis for the Global Ensemble Forecast System, version 12. *Mon. Wea. Rev.*, **150**, 59–79, https://doi.org/10.1175/MWR-D-21-0023.1.

Hamlet, A. F., D. Huppert, and D. P. Lettenmaier, 2002: Economic value of long-lead streamflow forecasts for Columbia River hydropower. *J. Water Resour. Plan. Manage.*, **128**, 91–101, https://doi.org/10.1061/(ASCE)0733-9496(2002)128:2(91).

Han, J., and H.-L. Pan, 2011: Revision of convection and vertical diffusion schemes in the NCEP Global Forecast System. *Wea. Forecasting*, **26**, 520–533, https://doi.org/10.1175/WAF-D-10-05038.1.

——, M. Witek, J. Teixeira, R. Sun, H.-L. Pan, J. K. Fletcher, and C. S. Bretherton, 2016: Implementation in the NCEP GFS of a hybrid eddy-diffusivity mass-flux (EDMF) boundary layer parameterization with dissipative heating and modified stable boundary layer mixing. *Wea. Forecasting*, **31**, 341–352, https://doi.org/10.1175/WAF-D-15-0053.1.

——, W. Wang, Y. C. Kwon, S.-Y. Hong, V. Tallapragada, and F. Yang, 2017: Updates in the NCEP GFS cumulus convection schemes with scale and aerosol awareness. *Wea. Forecasting*, **32**, 2005–2017, https://doi.org/10.1175/WAF-D-17-0046.1.

Harris, L. M., and S.-J. Lin, 2013: A two-way nested global-regional dynamical core on the cubed-sphere grid. *Mon. Wea. Rev.*, **141**, 283–306, https://doi.org/10.1175/MWR-D-11-00201.1.

Hazra, A., H. S. Chaudhari, S. K. Saha, and S. Pokhrel, 2017: Effect of cloud microphysics on Indian summer monsoon precipitating clouds: A coupled climate modeling study. *J. Geophys. Res. Atmos.*, **122**, 3786–3805, https://doi.org/10.1002/2016JD026106.

Hegerl, G. C., T. J. Crowley, M. Allen, W. T. Hyde, H. N. Pollack, J. Smerdon, and E. Zorita, 2007: Detection of human influence on a new, validated 1500-year temperature reconstruction. *J. Climate*, **20**, 650–666, https://doi.org/10.1175/JCLI4011.1.

Houze, R. A., 1997: Stratiform precipitation in regions of convection: A meteorological paradox? *Bull. Amer. Meteor. Soc.*, **78**, 2179–2196, https://doi.org/10.1175/1520-0477(1997)078<2179:SPIROC>2.0.CO;2.

Huang, L., and Y. L. Luo, 2017: Evaluation of quantitative precipitation forecasts by TIGGE ensembles for South China during the pre-summer rainy season. *J. Geophys. Res. Atmos.*, **122**, 8494–8516, https://doi.org/10.1002/2017JD026512.

Indira Rani, S. I., T. Arulalan, J. P. George, E. N. Rajagopal, R. Renshaw, A. Maycock, D. M. Barker, and M. Rajeevan, 2021: IMDAA: High-resolution satellite-era reanalysis for the Indian monsoon region. *J. Climate*, **34**, 5109–5133, https://doi.org/10.1175/JCLI-D-20-0412.1.

Jiang, M., and Coauthors, 2017: Potential influences of neglecting aerosol effects on the NCEP GFS precipitation forecast. *Atmos. Chem. Phys.*, **17**, 13 967–13 982, https://doi.org/10.5194/acp-17-13967-2017.

Jonkman, S. N., 2005: Global perspectives on loss of human life caused by floods. *Nat. Hazards*, **34**, 151–175, https://doi.org/10.1007/s11069-004-8891-3.

Kar, S. C., A. Hovsepyan, and C. K. Park, 2006: Economic values of the APCN multi-model ensemble categorical seasonal predictions. *Meteor. Appl.*, **13**, 267–277, https://doi.org/10.1017/S1350482706002271.

Keller, S., and A. Atzl, 2014: Mapping natural hazard impacts on road infrastructure—The extreme precipitation in Baden-Württemberg, Germany, June 2013. *Int. J. Disaster Risk Sci.*, **5**, 227–241, https://doi.org/10.1007/s13753-014-0026-1.

Krishna, R. P. M., S. A. Rao, A. Srivastava, H. P. Kottu, M. Pradhan, P. Pillai, R. A. Dandi, and C. T. Sabeerali, 2019: Impact of convective parameterization on the seasonal prediction skill of Indian summer monsoon. *Climate Dyn.*, **53**, 6227–6243, https://doi.org/10.1007/s00382-019-04921-y.

Krishnamurthy, C. K. B., U. Lall, and H.-H. Kwon, 2009: Changing frequency and intensity of rainfall extremes over India from 1951 to 2003. *J. Climate*, **22**, 4737–4746, https://doi.org/10.1175/2009JCLI2896.1.

Krishnamurti, T. N., A. Chakraborty, and A. K. Mishra, 2010: Improving multimodel forecasts of the vertical distribution of heating using the TRMM profiles. *J. Climate*, **23**, 1079–1094, https://doi.org/10.1175/2009JCLI2878.1.

Krishnan, R., A. D. Choudhury, R. Chattopadhyay, and M. Mujumdar, 2011: *Monsoon Simulation. IMD Monogr.*, No. 2, India Meteorological Department, 189–232.

Li, W., H. Guan, Y. Zhu, X. Zhou, B. Fu, D. Hou, E. Sinsky, and X. Xue, 2019: Prediction skill of the MJO, NAO and PNA in the NCEP FV3-GEFS 35-day experiments. *44th NOAA Annual Climate Diagnostics and Prediction Workshop*, Durham, NC, NOAA/National Weather Service, 4 pp., https://www.nws.noaa.gov/ost/climate/STIP/44CDPW/44cdpw-WLi.pdf.

Lin, S.-J., 2004: A "vertically Lagrangian" finite-volume dynamical core for global models. *Mon. Wea. Rev.*, **132**, 2293–2307, https://doi.org/10.1175/1520-0493(2004)132<2293:AVLFDC>2.0.CO;2.

——, and R. B. Rood, 1997: An explicit flux-form semi-Lagrangian shallow-water model on the sphere. *Quart. J. Roy. Meteor. Soc.*, **123**, 2477–2498, https://doi.org/10.1002/qj.49712354416.

Litta, A. J., B. Chakrapani, and V. Mohankumar, 2007: Mesoscale simulation of an extreme rainfall event over Mumbai, India, using a high-resolution MM5 model. *Meteor. Appl.*, **14**, 291–295, https://doi.org/10.1002/met.31.

Mahmood, S., J. Davie, P. Jermey, R. Renshaw, J. P. George, E. N. Rajagopal, and S. I. Rani, 2018: Indian monsoon data assimilation and analysis regional reanalysis: Configuration and performance. *Atmos. Sci. Lett.*, **19**, e808, https://doi.org/10.1002/asl.808.

Mason, S. J., 2004: On using "climatology" as a reference strategy in the Brier and ranked probability skill scores. *Mon. Wea. Rev.*, **132**, 1891–1895, https://doi.org/10.1175/1520-0493(2004)132<1891:OUCAAR>2.0.CO;2.

——, and N. E. Graham, 1999: Conditional probabilities, relative operating characteristics, and relative operating levels. *Wea. Forecasting*, **14**, 713–725, https://doi.org/10.1175/1520-0434(1999)014<0713:CPROCA>2.0.CO;2.

Mirza, M. M. Q., 2011: Climate change, flooding in South Asia and implications. *Reg. Environ. Change*, **11**(S1), 95–107, https://doi.org/10.1007/s10113-010-0184-7.

Mukherjee, A. K., 1980: Dimension of an offshore vortex in East Arabian Sea as deduced from observations during MONEX 1979: FGGE Operations Report. Vol. 9A, World Meteorological Organization, 176–184.

——, M. K. Rao, and K. C. Saha, 1978: Vortices embedded in the trough of low pressure off Maharashtra-Goa coasts during the month of July. *Mausam*, **29**, 61–65, https://doi.org/10.54302/mausam.v29i1.2859.

Mukhopadhyay, P., and Coauthors, 2019: Performance of a very high-resolution global forecast system model ($GFST_{1534}$) at 12.5 km over the Indian region during the 2016–2017 monsoon seasons. *J. Earth Syst. Sci.*, **128**, 155, https://doi.org/10.1007/s12040-019-1186-6.

Murphy, A. H., 1993: What is a good forecast? An essay on the nature of goodness in weather forecasting. *Wea. Forecasting*, **8**, 281–293, https://doi.org/10.1175/1520-0434(1993)008<0281:WIAGFA>2.0.CO;2.

Nageswararao, M. M., U. C. Mohanty, S. S. V. S. Ramakrishna, A. Nair, and S. K. Prasada, 2016: Characteristics of winter precipitation over Northwest India using high-resolution gridded dataset (1901–2013). *Global Planet. Change*, **147**, 67–85, https://doi.org/10.1016/j.gloplacha.2016.10.017.

——, M. C. Sannan, and U. C. Mohanty, 2019a: Characteristics of various rainfall events over South Peninsular India during northeast monsoon using high-resolution gridded dataset (1901–2016). *Theor. Appl. Climatol.*, **137**, 2573–2593, https://doi.org/10.1007/s00704-018-02755-y.

——, P. Sinha, U. C. Mohanty, R. K. Panda, and G. P. Dash, 2019b: Evaluation of district-level rainfall characteristics over Odisha using high-resolution gridded dataset (1901–2013). *SN Appl. Sci.*, **1**, 1211, https://doi.org/10.1007/s42452-019-1234-5.

Nayak, M. A., and S. Ghosh, 2013: Prediction of extreme rainfall event using weather pattern recognition and support vector machine classifier. *Theor. Appl. Climatol.*, **114**, 583–603, https://doi.org/10.1007/s00704-013-0867-3.

Palmer, T. N., and Coauthors, 2004: Development of a European Multimodel Ensemble System for Seasonal-to-Interannual Prediction (DEMETER). *Bull. Amer. Meteor. Soc.*, **85**, 853–872, https://doi.org/10.1175/BAMS-85-6-853.

——, R. Buizza, F. Doblas-Reyes, T. Jung, M. Leutbecher, G. Shutts, M. Steinheimer, and A. Weisheimer, 2009: Stochastic parametrization and model uncertainty. ECMWF Tech. Memo. 598, 42 pp., https://www.ecmwf.int/node/11577.

Pattanaik, D. R., 2007: Variability of convective activity over the north Indian Ocean and its impacts on monsoon rainfall over India. *Pure Appl. Geophys.*, **164**, 1527–1545, https://doi.org/10.1007/s00024-007-0243-2.

Piani, C., J. Haerter, and E. Coppola, 2010: Statistical bias correction for daily precipitation in regional climate models over Europe. *Theor. Appl. Climatol.*, **99**, 187–192, https://doi.org/10.1007/s00704-009-0134-9.

Pokhrel, S., A. Hazra, H. S. Chaudhari, S. K. Saha, F. Paulose, S. Krishna, R. Phani, and S. A. Rao, 2018: Hindcast skill improvement in Climate Forecast System (CFSv2) using modified cloud scheme. *Int. J. Climatol.*, **38**, 2994–3012, https://doi.org/10.1002/joc.5478.

Putman, W. M., and S.-J. Lin, 2007: Finite-volume transport on various cubed-sphere grids. *J. Comput. Phys.*, **227**, 55–78, https://doi.org/10.1016/j.jcp.2007.07.022.

Rajeevan, M., J. Bhate, and A. K. Jaswal, 2008: Analysis of variability and trends of extreme rainfall events over India using 104 years of gridded daily rainfall data. *Geophys. Res. Lett.*, **35**, L18707, https://doi.org/10.1029/2008GL035143.

Ramu, D. A., and Coauthors, 2016: Indian summer monsoon rainfall simulation and prediction skill in the CFSv2 coupled model: Impact of atmospheric horizontal resolution. *J.*

Geophys. Res. Atmos., **121**, 2205–2221, https://doi.org/10.1002/2015JD024629.

Rao, S. A., and Coauthors, 2019: Monsoon mission: A targeted activity to improve monsoon prediction across scales. *Bull. Amer. Meteor. Soc.*, **100**, 2509–2532, https://doi.org/10.1175/BAMS-D-17-0330.1.

Rao, Y. P., 1976: Southwest monsoon: Synoptic meteorology. *IMD Meteor. Monogr.*, No. 1/1976, India Meteorological Department, 367 pp.

Roebber, P. J., 2009: Visualizing multiple measures of forecast quality. *Wea. Forecasting*, **24**, 601–608, https://doi.org/10.1175/2008WAF2222159.1.

Rosenberg, E. A., P. W. Keys, D. B. Booth, D. Hartley, J. Burkey, A. C. Steinemann, and D. P. Lettenmaier, 2010: Precipitation extremes and the impacts of climate change on stormwater infrastructure in Washington State. *Climatic Change*, **102**, 319–349, https://doi.org/10.1007/s10584-010-9847-0.

Rosenfeld, D., U. Lohmann, G. B. Raga, C. D. O. Dowd, M. Kulmala, S. Fuzzi, A. Reissell, and M. O. Andreae, 2008: Flood or drought: How do aerosols affect precipitation? *Science*, **700**, 1309–1313, https://doi.org/10.1126/science.1160606.

Rosenzweig, C., F. N. Tubiello, R. Goldberg, E. Mills, and J. Bloomfield, 2002: Increased crop damage in the US from excess precipitation under climate change. *Global Environ. Change*, **12**, 197–202, https://doi.org/10.1016/S0959-3780(02)00008-0.

Routray, A., U. C. Mohanty, N. Dev, S. R. H. Rizvi, and K. K. Osuri, 2010: Simulation of heavy rainfall events over Indian monsoon region using WRF-3DVAR data assimilation system. *Meteor. Atmos. Phys.*, **106**, 107–125, https://doi.org/10.1007/s00703-009-0054-3.

Sagar, S. K., M. Rajeevan, S. Vijaya Bhaskara Rao, and A. K. Mitrac, 2017: Prediction skill of rainstorm events over India in the TIGGE weather prediction models. *Atmos. Res.*, **198**, 194–204, https://doi.org/10.1016/j.atmosres.2017.08.017.

Saha, S., and Coauthors, 2014: The NCEP Climate Forecast System version 2. *J. Climate*, **27**, 2185–2208, https://doi.org/10.1175/JCLI-D-12-00823.1.

——, A. Hazra, S. Pokhrel, H. S. Chaudhari, K. Sujith, A. Rai, H. Rahaman, and B. N. Goswami, 2019: Unraveling the mystery of Indian summer monsoon prediction: Improved estimate of predictability limit. *J. Geophys. Res. Atmos.*, **124**, 1962–1974, https://doi.org/10.1029/2018JD030082.

Satyanarayana, G. C. H., and S. C. Kar, 2016: Medium-range forecasts of extreme rainfall events during the Indian summer monsoon. *Meteor. Appl.*, **23**, 282–293, https://doi.org/10.1002/met.1553.

Sen Roy, S., and R. C. Balling Jr., 2004: Trends in extreme daily precipitation indices in India. *Int. J. Climatol.*, **24**, 457–466, https://doi.org/10.1002/joc.995.

Shutts, G., 2005: A kinetic energy backscatter algorithm for use in ensemble prediction systems. *Quart. J. Roy. Meteor. Soc.*, **131**, 3079–3102, https://doi.org/10.1256/qj.04.106.

——, and T. N. Palmer, 2004: The use of high-resolution numerical simulations of tropical circulation to calibrate stochastic physics schemes. *Proc. Workshop on Simulation and Prediction of Intra-Seasonal Variability with Emphasis on the MJO*, Reading, United Kingdom, ECMWF, 83–102, https://www.ecmwf.int/node/12212.

Sikka, D. R., 2006: A study on the monsoon low pressure systems over the Indian region and their relationship with drought and excess monsoon seasonal rainfall. COLA Tech. Rep., Vol. 217, 61 pp.

Soman, M. K., and K. Krishna Kumar, 1990: Some aspects of daily rainfall distributions over India during southwest monsoon season. *Int. J. Climatol.*, **10**, 299–311, https://doi.org/10.1002/joc.3370100307.

Stevens, B., and G. Feingold, 2009: Untangling aerosol effects on clouds and precipitation in a buffered system. *Nature*, **461**, 607–613, https://doi.org/10.1038/nature08281.

Stocker, T., Ed., 2011: Model hierarchy and simplified climate models. *Introduction to Climate Modelling*, Springer, 25–51.

Tao, W. K., J. P. Chen, Z. Li, C. Wang, and C. Zhang, 2012: Impact of aerosols on convective clouds and precipitation. *Rev. Geophys.*, **50**, RG2001, https://doi.org/10.1029/2011RG000369.

Toth, Z., O. Talagrand, G. Candille, and Y. Zhu, 2003: Probability and ensemble forecasts. *Forecast Verification: A Practitioner's Guide in Atmospheric Science*, I. T. Jolliffe and D. B. Stephenson, Eds., Wiley, 137–163.

Twomey, S. A., M. Piepgrass, and T. L. Wolfe, 1984: An assessment of the impact of pollution on global cloud albedo. *Tellus*, **36B**, 356–366, https://doi.org/10.3402/tellusb.v36i5.14916.

Vitart, F., W. Robertson, and D. L. T. Anderson, 2012: Subseasonal to seasonal prediction project: Bridging the gap between weather and climate. *WMO Bull.*, **61**, 23–28.

——, and Coauthors, 2017: The Subseasonal to Seasonal (S2S) prediction project database. *Bull. Amer. Meteor. Soc.*, **98**, 163–173, https://doi.org/10.1175/BAMS-D-16-0017.1.

Vogel, E., M. G. Donat, L. V. Alexander, M. Meinshausen, D. K. Ray, D. Karoly, N. Meinshausen, and K. Frieler, 2019: The effects of climate extremes on global agricultural yields. *Environ. Res. Lett.*, **14**, 054010, https://doi.org/10.1088/1748-9326/ab154b.

Wang, B., Q. Ding, and J.-G. Jhun, 2006: Trends in Seoul (1778–2004) summer precipitation. *Geophys. Res. Lett.*, **33**, L15803, https://doi.org/10.1029/2006GL026418.

Webster, P. J., and C. Hoyos, 2004: Prediction of monsoon rainfall and river discharge on 15–30-day time scales. *Bull. Amer. Meteor. Soc.*, **85**, 1745–1766, https://doi.org/10.1175/BAMS-85-11-1745.

Wheeler, M. C., H. Zhu, A. H. Sobel, D. Hudson, and F. Vitart, 2016: Seamless precipitation prediction skill comparison between two global models. *Quart. J. Roy. Meteor. Soc.*, **143**, 374–383, https://doi.org/10.1002/qj.2928.

Wilks, D. S., 2011: *Statistical Methods in the Atmospheric Sciences.* 3rd ed. International Geophysics Series, Vol. 100, Academic Press, 704 pp.

Wood, A. W., L. R. Leung, V. Sridhar, and D. Lettenmaier, 2004: Hydrologic implications of dynamical and statistical approaches to downscaling climate model outputs. *Climatic Change*, **62**, 189–216, https://doi.org/10.1023/B:CLIM.0000013685.99609.9e.

Yao, C., W. Qian, S. Yang, and Z. Lin, 2010: Regional features of precipitation over Asia and summer extreme precipitation over Southeast Asia and their associations with atmospheric-oceanic conditions. *Meteor. Atmos. Phys.*, **106**, 57–73, https://doi.org/10.1007/s00703-009-0052-5.

Zhai, P., X. Zhang, H. Wan, and X. Pan, 2005: Trends in total precipitation and frequency of daily precipitation extremes over China. *J. Climate*, **18**, 1096–1108, https://doi.org/10.1175/JCLI-3318.1.

Zhou, X., Y. Zhu, B. Fu, D. Hou, J. Peng, Y. Luo, and W. Li, 2019: The development of next NCEP Global Ensemble Forecast System. *43rd NOAA Annual Climate Diagnostics and Prediction Workshop (CDPW)*, Santa Barbara, CA, NOAA/National Weather Service, 159–163.

——, and Coauthors, 2022: The development of the NCEP Global Ensemble Forecast System version 12. *Wea. Forecasting*, https://doi.org/10.1175/WAF-D-21-0112.1, in press.

Zhu, Y., and Y. Luo, 2015: Precipitation calibration based on frequency matching method (FMM). *Wea. Forecasting*, **30**, 1109–1124, https://doi.org/10.1175/WAF-D-13-00049.1.

——, X. Zhou, M. Pena, W. Li, C. Melhauser, and D. Hou, 2017: Impact of sea surface temperature forcing on weeks 3 and 4 forecast skill in the NCEP Global Ensemble Forecast System. *Wea. Forecasting*, **32**, 2159–2174, https://doi.org/10.1175/WAF-D-17-0093.1.

——, and Coauthors, 2018: Toward the improvement of subseasonal prediction in the National Centers for Environmental Prediction Global Ensemble Forecast System. *J. Geophys. Res. Atmos.*, **123**, 6732–6745, https://doi.org/10.1029/2018JD028506.